Using Repeated Landau-Zener Transitions to Factor Integers with Superconducting Qubits

Jeffrey A. Grover

Advisor: Professor Jonathan R. Friedman
May 8, 2009

Submitted to the
Department of Physics of Amherst College
in partial fulfilment of the
requirements for the degree of
Bachelors of Arts with honors

Abstract

In 1994, Peter Shor demonstrated that quantum computers can efficiently factor large integers, a problem believed to be computationally difficult on classical computers. Despite the excitement created by this discovery, to date scientists have managed to factor only the number 15 using Shor's algorithm. The goal of this thesis is to explore an end-around method of factoring integers that is fundamentally different than that of Shor.

We consider a superconducting flux qubit as our two level system (though it can be extended to other implementations). The two lowest energy levels of this qubit have an energy splitting at the flux degeneracy point resulting in an avoided crossing. By initializing the qubit in its ground state and applying a harmonic driving flux, we can induce repeated Landau-Zener transitions into the excited state as the qubit passes the avoided crossing. This process is analogous to Mach-Zehnder interferometry and results in diffraction. If the drive frequency is a factor of the flux detuning (in appropriate units), then repeated the Landau-Zener transitions will yield constructive interference. As it stands, however, this method is a factor tester and not a factorizer. We are exploring different entanglement schemes that might allow us to test multiple factors simultaneously and produce the desired speedup.

Acknowledgments

My advisor since the first day of orientation, my professor for four of the physics classes I took and two others in which I was a TA, and now my thesis advisor, Professor Friedman deserves more thanks than I could hope to convey. It would be impossible to overstate your influence on my education, both within and beyond physics. As an advisor you always offered thoughtful advice on courses and on life and challenged me to step outside my comfort zone. As a physicist you taught by asking probing questions rather than easily divulging answers, a method I've come to appreciate more and more. Throughout this thesis you constantly prodded me to do less reading and more doing, and I hope that I've done enough to make you proud of my efforts.

I also want to thank the rest of the Friedman Lab - Max, Yiming, Katie, and Jim (and we still feel your presence, Eduardo) - for making this experience more fun than it would have been on my own. I know I was just the lonely theorist, but it was always nice to be able to come down to the lab for a chat, and I learned a lot from you guys in our weekly meetings.

I would like to thank the Physics Department for the close relationships I've formed with the other majors across years and for the stimulating but casual learning environment created by all of the professors. I would specfi-

cially like to thank Professor Hunter for introducing me to physics research (I know you often take jabs at theorists, so you'll be happy to know your efforts weren't wasted: I'm planning on going back to your side in graduate school). Jagu, you also deserve my sincerest appreciation for always offering a delicious, home-cooked meal and a friendly ear to listen to, well, anything. And though your stint here was too short, thanks, Russ, for your generous help with Mathematica.

I cannot forget the other half of my academic experience at Amherst: the math department. My other advisor and professor of another four of my courses (so really I've had only two professors here), Professor Benedetto epitomizes what I imagine the Amherst professor to be. Your lectures - if I can find time to breathe - are always interspersed with tidbits of information that set the greater context of math within the world, and your sometimes lengthy tangents are some of my favorite classroom moments. I haven't had a class with Professor Starr since my freshman year, but even after my dismal performance in Math 28 you haven't given up on me. Your influence has extended far beyond those first two math courses through the truckload of books you have donated to my collection and through the wonderful conversations we've shared. I hope that your newfound retirement will offer you some rest after a long career, but Amherst is losing one of its greats.

Going beyond Amherst, I can trace back my passion for science to my high school chemistry teacher, Mr. Corcoran (I still can't bring myself to call you Matthew... sorry). Though science has interested me for as long as I can remember, you ignited in me a desire to pursue it as a career. After this,

my umpteenth year of education, you still remain one of my best teachers, and your guidance persists years after I've left Framingham High through occasional books and continued friendship.

We live in filth, but my five roommates - Joe, Umang, Adam, Ben and Max - are five of my closest friends. Thank you for making this year unforgettable and keeping things interesting. We've still got a whiteboard's worth of activities to finish.

Joe, you're important enough to thank twice, so here's your second thank you. You're my best gob, and you've been one of my defining influences at Amherst. I'm continually thankful that you didn't get that RC position in South; that room in Williston was way too big to have all to myself. Sheah.

Emily, you've made this last semester of mine a refreshing one. Thanks for keeping me sane, even from afar.

And last, but the exact opposite of least, I want to thank my family: Mom, Dad, and Jill. Through thick and thin you've been my biggest supporters, even if communicating with me was like trying to hack into the NSA. I couldn't even begin to thank you for everything because I owe everything to you guys. I love you.

Contents

List of Figures

Chapter 1

Introduction

Quantum Mechanics and Computing

During a 1981 conference at MIT, Richard Feynman delivered a keynote speech titled "Simulating Physics with Computers," which first proposed the idea of a quantum computer [1]. In it he considered whether or not classical computers could efficiently simulate the physical world, and, indeed, he determined the task to be impossible. Carrying out such simulation would require a non-Turing processor that made use of the very laws it intended to calculate: a quantum computer. For about the next ten years, the field remained largely academic but grew steadily. In 1985 David Deutsch offered the first example of a quantum algorithm that would provide speedup over its classical counterpart [2], and he and Richard Jozsa extended his result to a much more general case in 1992 [3].

While Deutsch and Jozsa'a 1992 algorithm would become a fundamental

building block of later quantum algorithms, on its own it was still useless except as a scholarly pursuit. This changed in 1994 when Peter Shor, then at Bell Labs, developed a quantum factoring algorithm that could resolve an integer N into its prime factors in time $O((\log N)^3)$ [4]. Based on the calculation of the order of a function, a process that is equivalent to factor finding, Shor's algorithm exploits the ability of quantum states to be put into coherent superpositions. This allows single operations to simultaneously manipulate multiple states. An important discovery on its own, Shor's algorithm carried with it weighty practical implications. The security of public-key encryption rests on the belief that the factoring problem is a computationally difficult problem. A sufficiently large computer, if realized, holds the potential to break this method of encryption. In 1996, Lov Grover made a similarly landmark discovery. He constructed a quantum algorithm to search a database of N entries in time $O(N^{1/2})$, which provided quadratic speedup over classical linear search [5]. While the improvement is not exponential, quadratic speedup is quite dramatic for large N, and it can be proved that Grover's algorithm is the optimal quantum search algorithm. After Shor's and Grover's insights, a flood of government money and newfound interest accelerated the progress of quantum computing.

Over the last 15 years, much attention has been paid to the construction of a physical quantum computer, which has proven to be a challenging engineering problem. In order to maintain their "quantumness" long enough to carry out meaningful computations, quantum systems must be sufficiently isolated from the outside environment or else they will decohere. Another issue is

linking together more and more quantum bits in order to realize complicated algorithms.

A specific implementation of a quantum computer based on superconducting circuits exhibits shorter coherence times relative to other designs, but it holds greater promise in terms of scalability [6]. Their shorter coherence times result from the need to connect the superconductor circuits - devices that need temperatures on the order of mK to function properly - to electronics at room temperature. On the other hand, because we can print complicated superconducting circuits via electron-beam lithography, it is not impossible to piece together a large number of these circuits (less difficult than individually controlling a similar number of atoms, say). This method of quantum computation will be discussed in much more detail later, but here we wanted to give a general sense of the field.

Landau Zener Transitions and Quantum Computers

At first glance, Landau-Zener transitions do not appear to have much to do with quantum computing. Hopefully by the end of this introduction - and at the very least, this thesis - the connection will be much clearer.

In 1932, Landau [7], Zener [8], and Stückelberg [9] each calculated the probability that a particle in a potential with an avoided crossing would "jump" the crossing and make a nonadiabatic transition. Though they reduced the problem to a very specific case, their result has proved to be remarkably accurate in

approximating more complicated situations. As such, the Landau-Zener model has been a very successful predictor of the quantum dynamics of systems with avoided crossings.

The theory surrounding Landau-Zener transitions has been expanded through the study of extensions to N-level systems and the study of the effects of dissipation, for instance. Of particular interest was an in-depth investigation of sequential Landau-Zener transitions induced by some periodic drive about the anticrossing. In the early 1990s, Yosuke Kayanuma began studying repeated transitions and has continued this line of research through the present [10–15]. His work, along with the work of others [16], presented the interferometer-like nature of repeated transitions. Depending on how one controlled the phase accumulated between transitions, one could produce coherent population oscillations or completely quench them. This led Shytov *et al.* in 2003 to suggest repeated Landau-Zener transitions as a means for controlling the dynamics of a qubit. Specifically, they considered superconduting qubits, in which Izmalkov *et al.* observed Landau-Zener transitions a year later [17]. Since then repeated Landau-Zener transitions have been observed in charge [18–20] and flux [21–25] qubits. These experimental confirmations of the resulting interference from repeated Landau-Zener transitions have opened up a new method of manipulating qubits.

It is worth mentioning that even single Landau-Zener transitions play roles in quantum computing in two very contradictory ways. In 2002 Garanin and Schilling demonstrated that we can use the sweep through the avoided crossing to precisely determine the transition probability [26]. As a result, others

have proposed using Landau-Zener transitions as means for performing gate operations on qubits [27, 28]. Different groups have studied the potential of creating entangled states via Landau-Zener transitions in circuit QED architectures, where the qubit is coupled strongly to a microwave resonator on a circuit that behaves like a resonant cavity [29–31].

On the other side of the spectrum is adiabatic quantum computing, first proposed at the turn of the millenium [32]. In this model, the system is prepared in the quantum ground state and evolved adiabatically to a new Hamiltonian that encodes the answer to a problem. Because this evolution is done adiabatically, the system will remain in the ground state for the duration of the calculation. As the name "adiabatic quantum computing" suggests, a nonadiabatic process like a Landau-Zener transition is undesirable since it would take the system to the excited state. Thus there has been a substantial effort to study how to perform adiabatic quantum computing as quickly as possible without inducing a Landau-Zener transition [33, 34].

Diffraction and Factoring - A New Method?

In 1996, Clauser and Dowling saw a parallel between diffraction and factoring and explored the relationship in depth [35]. They found that if you use a simple N-slit interferometer, the diffraction pattern contains information about the wavelength of the light, the distance between slits, and the distance from the slits to the screen. If you relate those physical quantities to an integer, then you can use the diffraction pattern to determine whether or not that integer

is a factor of N. A year later, Summhammer built upon this method to create a factorization method using a Mach-Zehnder interferometer, encoding the factor information within the phase shift. Because these two schemes used only classical optics and did not take advantage of quantum entanglement, they did not achieve any speedup over known algorithms.

They did, however, inspire a small but active field of research concerning Gauss sum factorization that uses the principle of diffraction to test whether or not an integer is a factor of a given number [36]. To date, these newer methods have yet to exploit entanglement and thus have not demonstrated any computational advantages. But by combining repeated Landau-Zener transitions in superconducting qubits with factorization methods based on diffraction, we hope to present a new scheme that has the potential to do what previous attempts have failed to do. There remain many open questions concerning this proposal, but our preliminary results suggest that entanglement can be used to test two integers simultaneously, a key step in using diffraction-like phenomena to factor numbers.

The Organization of this Thesis

This thesis is structured as follows:

- Chapter 2 gives a brief and general overview of quantum computing, outlining the basic properties of qubits. We discuss basic quantum logic, including single- and mutliple-qubit gates, as well as the first quantum algorithm to show speedup over its classical analogue. The chapter serves

to give context to the field in general.

- Chapter 3 develops a specific physical implementation of a quantum two level system, the superconducting flux qubit. While the overall treatment is somewhat superficial, the message that a superconducting ring interrupted by a Josephson junction can act as a qubit is of fundamental importance. Much of the later discussion about Landau-Zener transitions hinges on the avoided crossing, which arises from the tunnel splitting between the two wells of the system's potential.

- Chapter 4 provides an in-depth look at Landau-Zener transitions, starting with the problem as first posed by Zener in 1932. We then turn to the issue of carrying out many Landau-Zener transitions in sequence, which can be thought of as a phase-dependent interference effect.

- Chapter 5 presents our factorization scheme in detail, but first offers an overview of the Clauser and Dowling and the Summhammer results to set the context of the method. We relate repeated Landau-Zener transitions to a Mach-Zehnder interferometer and present the MIT group's derivation of an analytical expression for the probability of switching to the excited state. We then use the resulting resonance condition as a means of testing factors, and use the switching probability to derive a scaling law. The chapter - and the thesis - concludes with a discussion of a coupling scheme that would allow for the simultaneous testing of multiple factors.

Chapter 2

Quantum Computing

This chapter[1] serves to introduce the reader to the basics of quantum computation and quantum information. While a brief description of the qubit might be sufficient to understand the quantum computing aspects of this thesis, a review of the basic concepts is necessary to set the context for why such a thesis might be important. Quantum computers, if realized, hold the potential to outperform their classical counterparts in nontrivial ways. This chapter aims to lay down the groundwork so that the reader can appreciate the origins of this potential.

[1]The results presented in this chapter are basic and now can be found in many sources. I will thus refrain from citing each individual formula and instead direct the reader to [37] and [38], from which most of the material was learned. In the case of specific algorithms, I will cite the original work even if nicer explanations might exist elsewhere.

2.1 Quantum Bits

We are all familiar with classical information in which the fundamental unit is a *bit*: 0 or 1, on or off, up or down. With bits, there is no in-between; they can occupy only one position at a given moment. Thus while N bits in a computer can represent 2^N different values, only one of those values is accessible at a time. Quantum information, however, flies in the face of this restriction as we will see in the next few sections.

2.1.1 Superposition

Let us start with an arbitrary quantum state $|\psi\rangle$ in a Hilbert (complete, complex inner product) space of arbitrary dimension. If we have a set of basis states for this space, $\{|\phi_i\rangle\}_{i\in\mathbb{Z}^+}$, the law of quantum superposition of states says that we can represent $|\psi\rangle$ as a linear combination of these basis states: $|\Psi\rangle = \sum_i a_i |\phi_i\rangle$, where are the a_i's are complex coefficient satisfying

$$|a_1|^2 + |a_2|^2 + \cdots = 1\,. \tag{2.1}$$

A quantum bit, or *qubit* for short, is simply a quantum state that resides in a two-dimensional Hilbert space. Thus we can define the basis states for this space to be $|0\rangle$ and $|1\rangle$, which we call the computational basis. An arbitrary state can then be represented as

$$|\psi\rangle = \alpha\,|0\rangle + \beta\,|1\rangle\ , \tag{2.2}$$

where α and β obey Eq. (2.1). This highlights a fundamental difference of classical and quantum computing. Rather than be only either $|0\rangle$ or $|1\rangle$, a qubit can take on infinitely many superpositions, and we can view it as a unit vector (more on that in the next section).

Of course, not all of these possible superpositions are accessible to us. If we perform a measurement on a quantum state in the 0-1 basis, the *measurement postulate* says that we will obtain either 0 or 1 with probability $|\alpha|^2$ or $|\beta|^2$, respectively, and that the state will then occupy the basis state whose output we measure. In this way we can view α and β as amplitudes for the two qubit basis states.

2.1.2 The Bloch Sphere

As mentioned above, a qubit is a vector in a complex vector space. A useful way to visualize a qubit then is a 3-dimensional representation called the *Bloch sphere*. Noting that the amplitudes satisfy Eq. (2.1), we can rewrite Eq. (2.2) as

$$|\psi\rangle = \cos\left(\frac{\theta}{2}\right)|0\rangle + e^{i\varphi}\sin\left(\frac{\theta}{2}\right)|1\rangle \ , \tag{2.3}$$

with θ being the azimuthal angle and φ the polar angle, as in Fig 2.1. Thus a qubit can be thought of as a vector pointing to a point on the Bloch sphere defined by θ and φ, with $|0\rangle$ and $|1\rangle$ lying along the positive and negative z-axis, respectively.

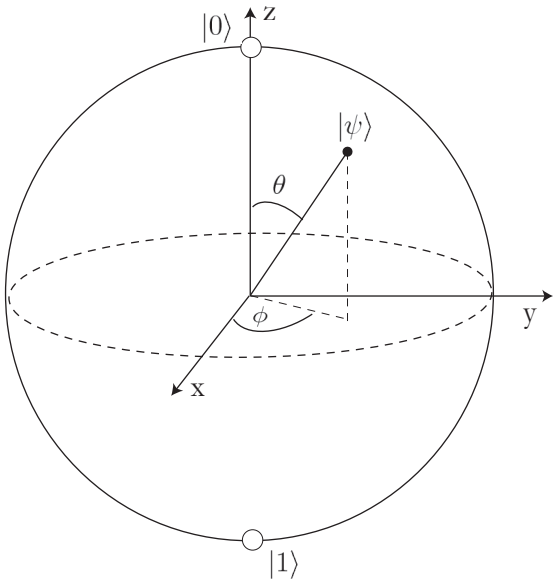

Figure 2.1: The Bloch sphere representation of a qubit.

2.1.3 Hilbert Space and Composite Systems

We have seen that a qubit lives in a 2-dimensional Hilbert space, but what happens if we have two qubits together? Consider two Hilbert spaces $\mathcal{H}_1$, $\mathcal{H}_2$ and two states $|\psi_1\rangle \in \mathcal{H}_1$, $|\psi_2\rangle \in \mathcal{H}_2$. Then the new state $|\psi_1\rangle \otimes |\psi_2\rangle$ lives in the space $\mathcal{H}_1 \otimes \mathcal{H}_2$, where $\otimes$ denotes the tensor product. This new space is large, having dimension $\dim(\mathcal{H}_1) \times \dim(\mathcal{H}_1)$ (see Appendix A).

As an important example, we look at the general case of two unentangled (to be defined in the next section) qubits, $|\psi\rangle = \alpha_0 |0\rangle + \alpha_1 |1\rangle$ and $|\phi\rangle = \beta_0 |0\rangle + \beta_1 |1\rangle$. For convenience we will from now on use the following notation to represent composite states:

$$|\psi\rangle \otimes |\phi\rangle \equiv |\psi\rangle |\phi\rangle \equiv |\psi\phi\rangle \ .$$

Thus we have

$$|\psi\rangle |\phi\rangle = \alpha_0\beta_0 |00\rangle + \alpha_0\beta_1 |01\rangle + \alpha_1\beta_0 |10\rangle + \alpha_1\beta_1 |11\rangle . \tag{2.4}$$

This illustrates how the size of a Hilbert space grows as we add more qubits. In general, for a N-qubit system, the associated Hilbert space will have dimension 2^N. As a result, a single state in this space encodes information about 2^N different computational basis states! This is where quantum computing draws some of its power over classical computing: with one operation we can simultaneously change the characteristics of many different states.

2.1.4 Entanglement

The state in Eq. (2.4) is nice because we can easily factor it into the tensor product of two pure states (by which we mean that all constituents of the system can be described by a single state vector). If, however, a state in a composite system cannot be written as a tensor product of states in the component systems, then that state is said to be *entangled*. The entangled qubits are thus inextricably linked: if I perturb one qubit I necessarily perturb the other. This purely quantum characteristic has some fanastic applications like teleportation [39] and provides some quantum algorithms exponential speedup over their classical analogues.

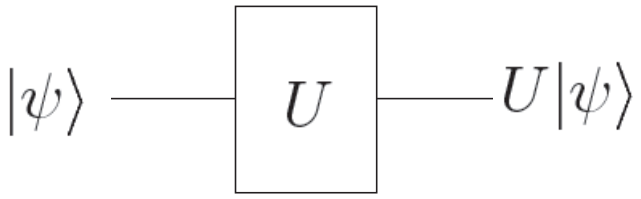

Figure 2.2: A circuit diagram illustrating a generic gate acting on a quantum state.

2.2 Quantum Logic

Given this description of quantum information and some of its basic properties, we now turn to the issue of manipulating this information. Just as classical computers possess a logic based on a set of gates and operations, so, too, do quantum computers. In this section we present a systematic treatment of quantum computation, which is known as the *quantum circuit model*.[2] This name is very descriptive: we actually envision qubit states traveling down wires in a circuit where they will pass through various arrays of gates (see Fig. 2.2). We can therefore visualize algorithms by drawing equivalent circuit diagrams. In these diagrams, time is assumed to flow from left to right, and each wire carries only one logical qubit.

2.2.1 Single-Qubit Gates

In Section 2.1.2 we recast the qubit as a unit vector ending at a point on the Bloch sphere embedded in $\mathbb{R}^3$. This is a helpful picture to have when imagining how quantum gates act on qubits: they rotate a qubit's state vector

[2]N.B.: There do exist *other* models of quantum computation such as cluster-state [40] and adiabatic quantum computing [32]. We have already mentioned the latter, in which Landau-Zener transitions are errors.

in the Bloch sphere. More rigorously, we define a quantum gate to be a unitary operator U:

$$UU^\dagger = I\,, \tag{2.5}$$

where $U^\dagger$ is the adjoint of U. In terms of the matrix reprenstation of U, $\dagger$ signifies the conjugate transpose of that matrix. We use unitary operators as gates because they preserve inner products and allow for the reversibility of quantum gate operations.

We now introduce a set of operators important to quantum computing, the Pauli operators (which, when grouped with the 2×2 identity matrix, form a basis for the 2-dimensional Hilbert space in which qubits live):

$$\sigma_x = \begin{pmatrix} 0 & 1 \\ 1 & 0 \end{pmatrix}\,,\ \sigma_y = \begin{pmatrix} 0 & -i \\ i & 0 \end{pmatrix}\,,\ \sigma_x = \begin{pmatrix} 1 & 0 \\ 0 & -1 \end{pmatrix}\,. \tag{2.6}$$

Within the Bloch sphere picture, the effect of σ_x, for instance, is to rotate a qubit by an angle π about the x-axis. Thus it can be viewed as a quantum version of a NOT gate, taking $|0\rangle$ to $|1\rangle$ and vice versa. More general rotations can be constructed out of the Pauli matrices by exponentiating the operators:

$$R_i = e^{\frac{-i\theta\sigma_i}{2}}, \tag{2.7}$$

which represents a roation by an angle θ about an axis i. One can use this technique to construct a rotation about any arbitrary axis. It can then be shown that any unitary operation on a single qubit can be written as a series of rotations. In this way we can visualize *all* single-qubit gate operations as

rotations of qubits within the Bloch sphere. The picture breaks down for two-qubit gates as they result in entangled states, which cannot be represented on the Bloch sphere.

It is also worth mentioning another single-qubit gate that is of fundamental importance to quantum computing algorithms. Called the Hadamard gate, it is given by the following matrix representation:

$$\frac{1}{\sqrt{2}} \begin{pmatrix} 1 & 1 \\ 1 & -1 \end{pmatrix} . \tag{2.8}$$

It acts on the computational basis states like a beamsplitter, creating equal superpositions of the basis states (with a relative phase of $e^{-i\pi}$ if the input is $|1\rangle$). Fig. 2.3 gives a Bloch sphere visualization of the Hadamard gate acting on the state $|0\rangle$.[3]

Before turning to multiple-qubit gates, we pause to make a comment about single-qubit gates within a multi-qubit system. If we have n qubits but want an operation Z to act on the i^{th} qubit without affecting the others, we must construct the gate as follows:

$$\underbrace{I \otimes \cdots \otimes I}_{i-1 \text{ times}} \otimes Z \otimes \underbrace{I \otimes \cdots \otimes I}_{n-i \text{ times}} , \tag{2.9}$$

where I is the 2×2 identity matrix. In an n-qubit system, then, it takes a $2^n \times 2^n$ matrix to represent a gate operation, making classical simulation of

[3]The Mathematica code for these figures has been adapted from
http://www.quantumscience.info/node/387 and
http://forums.wolfram.com/mathgroup/archive/1998/Mar/msg00102.html .

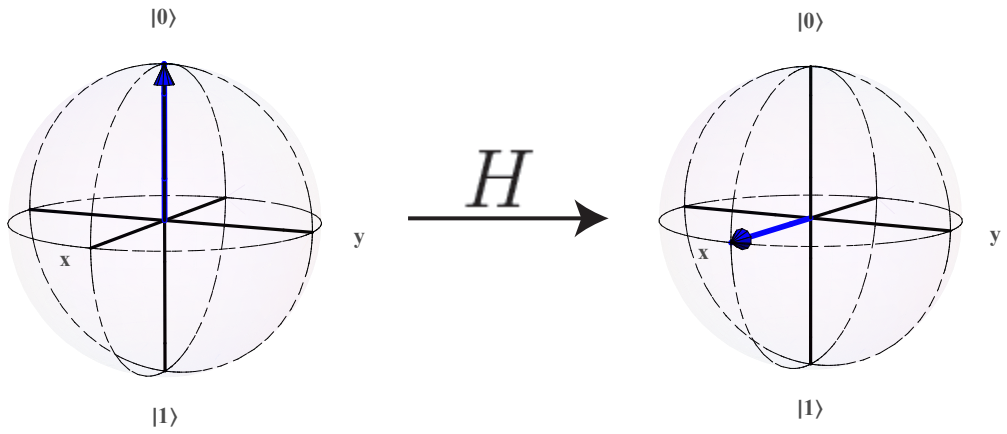

Figure 2.3: Bloch sphere representation of Hadamard taking $|0\rangle$ to $\frac{1}{\sqrt{2}}(|0\rangle + |1\rangle)$.

quantum computing difficult.

2.2.2 Multiple-Qubit Gates

While three-qubit gates such as the Toffoli gate exist, we restrict our attention here to two-qubit gates. Most often we want to alter one qubit (the *target* qubit) based on the state of another qubit (the *control* qubit). To do this we introduce controlled-U gates. These perform the unitary operation U on the target qubit if the state of the control qubit is $|1\rangle$ and leave the target qubit alone if the control is in state $|0\rangle$. One of the most important of these gates is the suggestively named controlled-NOT (CNOT) gate. For this gate the unitary operation is just NOT (i.e. it takes $|0\rangle$ to $|1\rangle$ and vice versa), and the gate behaves like a quantum version of XOR. Fig. 2.4 provides one example of the CNOT's function. Its importance stems from the fact that the set of gates CNOT, Hadamard, and phase (i.e. a gate that gives a qubit a relative

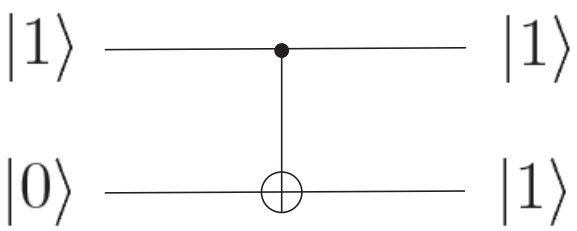

Figure 2.4: An example of the CNOT gate performing a controlled operation on two qubits.

phase) consistute a universal set of gates (see, e.g., [37]).

2.3 A Sample Algorithm

To illustrate the power of quantum computing, we turn to the first quantum algorithm to demonstrate speedup over any classical algorithm. Suppose we are given a binary function $f : \{0,1\} \to \{0,1\}$, and we want to know if the function is constant or balanced, i.e. if all the outputs are either 0 or 1 (constant), or if half the inputs yield 0 and the other half yield 1 (balanced). For instance, the function that maps 0 to 0 and 1 to 0 is said to be constant. Classically, you need to evaluate the function twice, namely $f(0)$ and $f(1)$ in order to determine this global property of the function with certainty. In 1985, however, David Deutsch showed [2] that a quantum computer will obtain the answer with only one query (in 1992 he and Richard Jozsa extended [3] this problem to the case of n inputs: $f : \{0,1\}^n \to \{0,1\}$). This is a toy problem with little physical significance, but it illustrates the power of quantum interference. The generalized algorithm of Deutsch-Jozsa also inspired the more applicable factorization scheme of Shor, among others [37].

Suppose we start with the input state $|\psi_0\rangle = |01\rangle$, meaning the first qubit is in state $|0\rangle$ and the second qubit is in state $|1\rangle$. We then send each qubit through a Hadamard gate to produce the state

$$|\psi_1\rangle = \left[\frac{|0\rangle + |1\rangle}{\sqrt{2}}\right]\left[\frac{|0\rangle - |1\rangle}{\sqrt{2}}\right] . \tag{2.10}$$

Now we must define a unitary operator U_f such that, given a binary function f (like the one given in the statement of the probelm), it performs the following map:

$$|x, y\rangle \xrightarrow{U_f} |x, y \oplus f(x)\rangle \ , \tag{2.11}$$

where $\oplus$ is addition mod 2. U_f acts on the state $|x\rangle\left(\frac{|0\rangle-|1\rangle}{\sqrt{2}}\right)$ in the following manner:

$$\begin{aligned} U_f : |x\rangle\left(\frac{|0\rangle - |1\rangle}{\sqrt{2}}\right) &\longmapsto \left(\frac{U_f\,|x\rangle\,|0\rangle - U_f\,|x\rangle\,|1\rangle}{\sqrt{2}}\right) \\ &= |x\rangle\left(\frac{|0 \oplus f(x)\rangle - |1 \oplus f(x)\rangle}{\sqrt{2}}\right) . \end{aligned} \tag{2.12}$$

If $f(x) = 0$, the state of the second qubit in Eq. (2.12) will remain unchanged. If, on the other hand, $f(x) = 1$, the second qubit's state will acquire an overall minus sign. Thus our original state develops a phase given by $(-1)^{f(x)}$, and the action of U_f is

$$U_f : |x\rangle\left(\frac{|0\rangle - |1\rangle}{\sqrt{2}}\right) \longmapsto (-1)^{f(x)}\,|x\rangle\left(\frac{|0\rangle - |1\rangle}{\sqrt{2}}\right) . \tag{2.13}$$

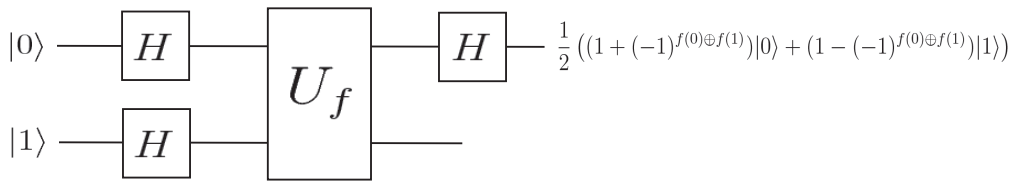

Figure 2.5: A quantum circuit for Deutsch's algorithm.

We now see that, after some manipulation, the state in Eq. (2.10) becomes

$$(-1)^{f(0)}\left(\frac{|0\rangle + (-1)^{f(0)\oplus f(1)}\,|1\rangle}{\sqrt{2}}\right)\left(\frac{|0\rangle - |1\rangle}{\sqrt{2}}\right). \tag{2.14}$$

So, if f is constant function, then we have $f(0) \oplus f(1) = 0$, and a final Hadamard gate on the first qubit will put it into state $|0\rangle$. Similarly, if f is balanced ($f(0)\oplus f(1) = 1$), then the Hadamard gate will put the first qubit into state $|1\rangle$. Thus to determine a *global* property of a function f, we perform the described operations and carry out only one measurement of the first qubit's state. The circuit diagram for this algorithm is displayed in Fig. 2.5.

While the improvement from two queries to one query may not seem significant, the worst-case number of evaluations for a classical n-bit system is $2^{n-1} + 1$ whereas the quantum analogue again requires only one [3]. This simple algorithm also illustrates the interpretation of quantum computers as interferometers [41], an elegant way to conceptualize how quantum computers manipulate information.

Chapter 3

Superconducting Qubits

Until now our discussion of qubits has been purely abstract. If we have any hope of constructing a quantum computer, however, we better be able to physically realize a quantum two-level system. While many such systems exist in nature (e.g., the spin of an electron), their existence does not automatically guarantee their usefulness as a quantum computing architecture. In order to be viable sources of information manipulation, these physical qubits must be scalable and possess long coherence times, among other properties [42]. Scientists have been able to engineer qubits that satisfy these criteria using quantum systems such as trapped ions [43], photons [44], and molecules (manipulated via NMR) [45]. Since these are examples of microscopic quantum systems, their applicability to quantum computing is not surprising. In addition to these implementations, however, physicists have created qubits out of genuinely macroscopic objects. In the late 1990s, two groups detected the superposition of distinct charge states in a Josephson junction circuit [46–48].

Then in 2000, Friedman *et al.* [49] and van der Wal *et al.* [50] demonstrated that *s*uperconducting *qu*antum *i*nterference *d*evices (SQUIDs) could be put into superpositions of flux states, with macroscopic supercurrents flowing in two directions simultaneously. These results confirmed that superconducting circuits could be used as qubits despite being macroscopic objects.

We direct our focus to this type of qubit.[1] This chapter will develop the superconducting qubit, focusing specifically on how we can create a two-level system out of two distinct flux states. The associated avoided crossing will motivate our exploration of Landau-Zener transitions in this system, which will consume most of this thesis.

3.1 Josephson Junctions

When its temperature drops below a critical value, T_C, a superconductor will exhibit strange properties such as perfect conductivity (allowing for persistent currents), the Meissner effect, and flux quantization [51]. Described by the BCS theory, these phenomena are the result of pairs of electrons forming Cooper pairs and condensing into a single quantum state [52]. Because of this condensation, the Cooper pairs are all characterized by one wavefunction with an associated phase. If we place a thin, insulating barrier between two superconductors, then each superconductor on either side of the barrier will have its own phase. We can therefore define a gauge-invariant phase difference, φ, across the barrier [53]. This setup, an insulator sandwiched between

[1] It should be noted, however, that Landau-Zener transitions have been observed in many systems and that the ideas presented here are perhaps extendable to other implementations.

two superconducting electrodes, constitutes a Josephson junction. It possesses two peculiar properties, a phase-dependent supercurrent and phase evolution based on an applied voltage:

$$I_S = I_C \sin\varphi \,, \tag{3.1}$$

$$\dot{\varphi} = \frac{2e}{\hbar} V = \frac{2\pi}{\Phi_0} \,, \tag{3.2}$$

where I_C is the critical current of the junction, and Φ_0 is the flux quantum, defined to be $h/2e$ from the quantization of flux in superconductors. These two phenomena are the result of tunneling of Cooper pairs through the junction barrier.

It is useful to create an equivalent circuit model for the Josephson junction, where we view it as a junction shunted by a capacitance C and resistance R. This is referred to as the resistively and capacitively shunted junction (RCSJ) model, and it provides us with an equation of motion for the circuit (assuming 0 bias current) [52]:

$$I_C \sin\varphi + V/R + C\dot{V} = 0 \,. \tag{3.3}$$

Each term represents the current through each of the three circuit elements of the RCSJ model of a junction. Since the elements are in parallel, Kirchoff's law implies that their sum is equal to the total current through the junction, which we take to be zero here. Substituting in the Josepshon relations Eqs. (3.1) and (3.2), this equation describes a particle of mass C within a potential

$$U(\varphi) = -E_J \cos\varphi \,, \tag{3.4}$$

where E_J is the Josephson energy of the junction and is given by $I_C\Phi_0/2\pi$ (see Fig. 3.1). Because of the presence of a capacticance between the two electrodes, we also define an associated charging energy of the junction given by

$$E_C = e^2/2C\,. \tag{3.5}$$

From now on we assume that $E_J \gg E_C$, so that phase (hence, as we will see later, flux) is the appropriate quantum variable (as opposed to charge). Note that adding a bias current to Eq. (3.3) is equivalent to adding a drive force to the particle. In terms of the potential, the current term results in an additional term linear in ϕ that tilts the potential. Thus this model is often referred to the tilted-washboard model [52]. If the bias current is less than the critical current, then the particle will remain in a potential well. Once this current is surpassed, however, the tilt increases enough to allow the particle to run down the potential, as in Fig. 3.1.

3.2 rf SQUIDs

Connecting the electrodes of a Josephson junction creates an inductive ring of superconductor interrupted by a barrier. This loop now has an associated self-inductance, L, and allows for magnetic flux, Φ_x, to be threaded through it (see Fig. 3.2). For historical reasons, this system is known as an rf SQUID. A varying dc flux through the ring changes the Q of the circuit, allowing one to measure the resultant change in flux. It is a peculiar feature of superconductors that the flux through any hole of a superconductor must be quantized in

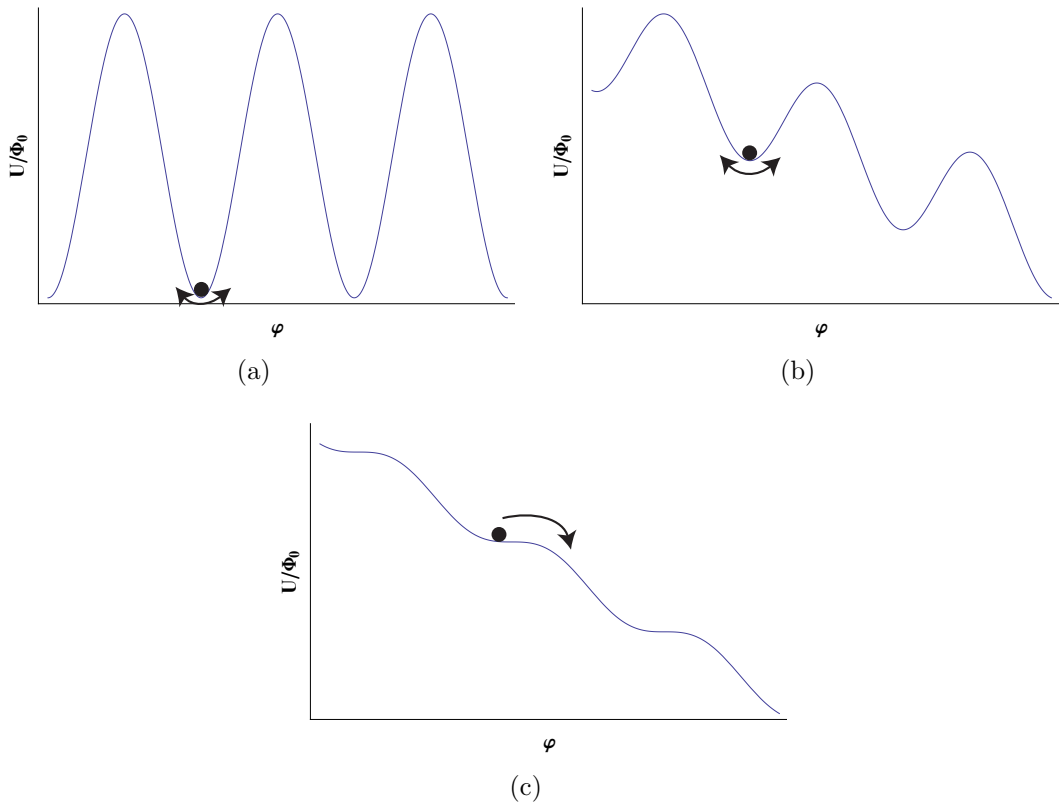

Figure 3.1: A particle in the tilted washboard potential with different bias currents: (a) $I/I_C = 0$, (b) $I/I_C = 0.2$, and (c) $I/I_C = 1$. Once the bias current reaches I_C, the particle can escape its well and roll down the potential.

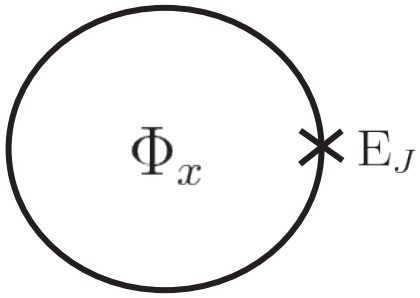

Figure 3.2: Circuit representation of a SQUID.

integer multiples of Φ_0. From this flux quantization, we can relate the total flux enclosed in the loop to the gauge-invariant phase of the junction by

$$\varphi = \frac{2\pi\Phi}{\Phi_0} \mod 2\pi \,, \tag{3.6}$$

where Φ is the total enclosed flux. We can substitute this value for φ into Eq. (3.1) to obtain a flux-dependent supercurrent:

$$I_S = I_C \sin\left(\frac{2\pi\Phi}{\Phi_0}\right) . \tag{3.7}$$

With Eq. (3.7) in hand we can recast the energy of the junction in this circuit, (3.4), in terms of the loop's flux as well.

Noting that the energy stored in an inductor can be written as

$$\frac{1}{2}LI^2 \,, \tag{3.8}$$

where I is the current flowing through the loop, we see the total potential of the system will have an added contribution due to this inductive energy. This can be further manipulated by writing the total flux in the inductor as the sum of the applied flux and the flux due to the current, LI:

$$\Phi = \Phi_x + LI \,. \tag{3.9}$$

Solving for LI, the inductive energy in Eq. (3.8) then becomes

$$\frac{(\Phi - \Phi_x)^2}{2L} \,, \tag{3.10}$$

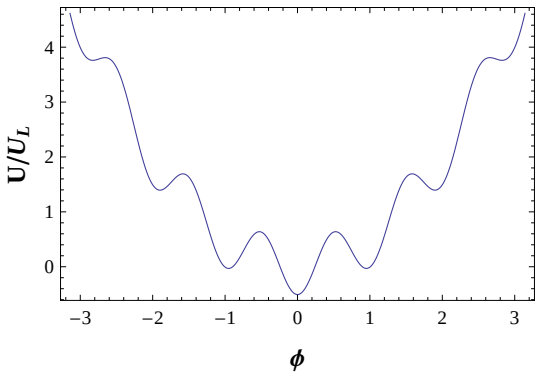

Figure 3.3: Potential energy of a SQUID with $\beta_L = 20$ and no applied external flux.

and we can add this to the junction's potential energy to obtain the total potential of the SQUID system [54]:

$$U(\Phi) = \frac{(\Phi - \Phi_x)^2}{2L} - E_J \cos\left(\frac{2\pi\Phi}{\Phi_0}\right) . \tag{3.11}$$

To better understand the properties of this potential, it is useful to reexpress it in terms of normalized variables $\phi \equiv \Phi/\Phi_0$ and $\phi_x \equiv \Phi_x/\Phi_0$ [49, 54]:

$$U(\phi) = U_L \left[\frac{1}{2}(\phi - \phi_x)^2 - \frac{\beta_L}{4\pi^2}\cos(2\pi\phi)\right] . \tag{3.12}$$

Here we've introduced the parameters $U_L \equiv \Phi_0^2/L$ and $\beta_L \equiv 2\pi L I_C/\Phi_0$. The former is simply a multiplicative factor and determines the energy scale of the potential, whereas the latter affects the potential's shape. The potential possesses two components, a quadratic term and a sinusoidal term. Considering these two terms together, we qualitatively expect the potential to be a parabola with oscillations in it (see Fig. 3.3). If the self-inductance is sufficiently large (so that β_L is larger than but on the order of unity) and ϕ_x is

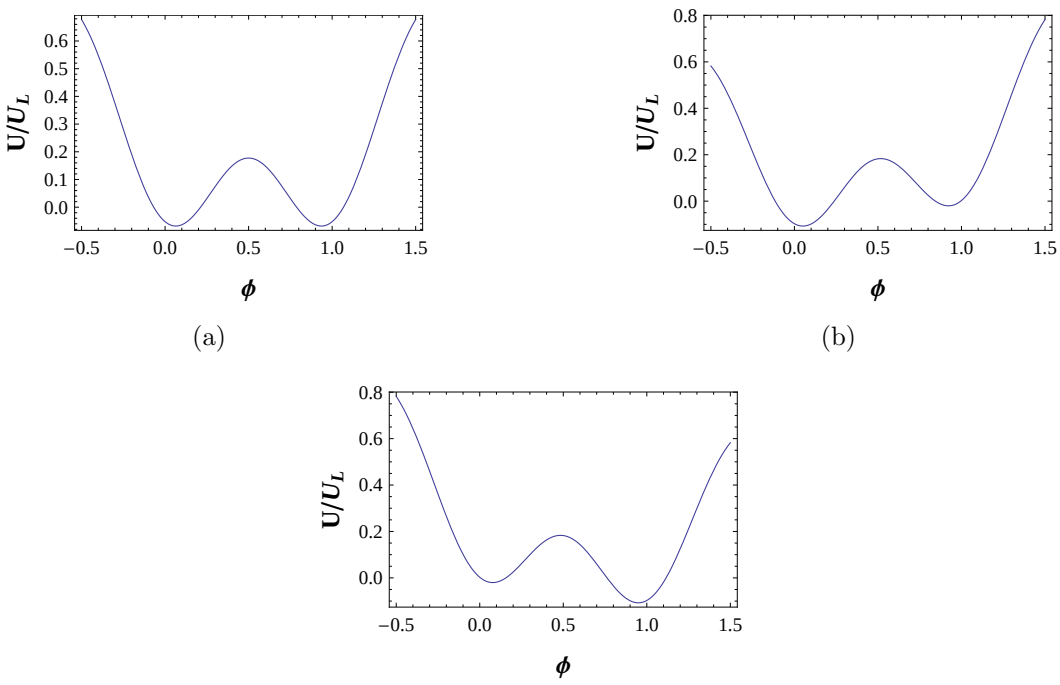

Figure 3.4: Potential energy plots showing the effect of different values of applied flux on symmetry (all with $\beta_L = 7$): (a) $\phi_x = 0.5$, (b) $\phi_x = 0.4$, and (c) $\phi_x = 0.6$.

near 1/2, the potential forms a double-well potential about $\phi = 1/2$ with a barrier dependent on U_L and β_L [6]. Each well represents a well-defined flux state of the SQUID corresponding to flux pointing either down or up in the loop. Because a flux through a loop causes current to flow, we can think of the flux states in terms of supercurrent flowing in either the counterclockwise or clockwise directions. Fig. 3.4 illustrates that when ϕ_x is equal to 1/2, the double well is symmetric and that varying ϕ_x tilts the potential. This produces an energy difference (denoted ε) between the two wells that can be shown to

be linear in the deviation of ϕ_x from 1/2 [54]:

$$\varepsilon \backsimeq U_L \Delta\phi_m(\phi_x - 1/2)\,, \tag{3.13}$$

where $\Delta\phi_m$ is the distance between the two wells. To put this difference in terms of a measurable quantity, we write it as a function of the persistent current, I_p, in the SQUID [50]:

$$\varepsilon = 2I_p\Phi_0(\phi_x - 1/2)\,. \tag{3.14}$$

This energy difference will be important when we discuss the two-level system within the qubit.

Now that the SQUID potential is fully defined, we turn to its Hamiltonian. Recalling the RCSJ model of a junction, there was an equivalent mass in the equation of motion determined by the capacticance, C. Its formula suggests that this term arises from charge stored on the junction's capacitor. We can think of this as having an associated kinetic energy term given by the charging energy from Eq. (3.5):

$$E_C = \frac{Q^2}{2C}\,. \tag{3.15}$$

We have replaced e with Q to represent the total charge on the capacitor as an operator $Q = -i\hbar\partial/\partial\Phi$ [6]. Thus Q is the conjugate momentum to flux, satisfying the commutation relation

$$[\Phi, Q] = i\hbar\,. \tag{3.16}$$

Combining Eqs. (3.11) and (3.15) we obtain the total Hamiltonian for the system:

$$H(\Phi) = \frac{Q^2}{2C} + \frac{(\Phi - \Phi_x)^2}{2L} - E_J \cos\left(\frac{2\pi\Phi}{\Phi_0}\right). \tag{3.17}$$

In general the Schrödinger equation for this Hamiltonian cannot be solved analytically. The periodic term of the potential energy suggests an energy band structure by the Bloch theorem. Indeed, if the quadratic term were not present, the energy eigenstates would be bands determined analytically by Mathieu functions (see, e.g., [53, 55]).

As is the case with any differential equation, however, we can solve for the eigenstates and eigenfunctions numerically, and this system has been studied extensively through diagonalization techniques [56, 57]. These simulations reveal a more complex structure than the Mathieu functions of a simple periodic potential. The authors also calculate the wavefunctions of the lowest energy levels and show that these states remain localized in the wells due to the quadratic term in the Hamiltonian. A key feature of the wavefunctions for flux values near the symmetry point of the potential is that they exhibit a superposition of states. In the next section we examine the system around the symmetry point, which will allow us to explain why this property of the wavefunctions arises. In fact, the apparent complexity of the energy levels becomes unimportant if we restrict our problem to flux values near $\Phi = \Phi_0/2$ and temperatures small enough such that our system occupies only the lowest energy states in either well [6]. This reduces the system to a two-level one that is easily solvable. Moreover, this suggests that we can use the flux states of a SQUID as our qubit. Given that we have produced a macroscopic electric

circuit to exhibit two-state quantum properties, we often refer to such systems as artificial atoms.

3.3 SQUID Two-Level System

We now consider the situation described above: our potential consists of two wells each with only one occupiable state. These states correspond to different flux states or, analogously, to persistent currents flowing in opposite directions. Let us denote the states in the left and right wells by $|L\rangle$ and $|R\rangle$, respectively. If we apply an external flux that is just less than $\Phi_0/2$, the wells tilt such that $|L\rangle$ is the energetically favored state. In the absence of tunneling, Eq. (3.14) implies that continuously increasing the external applied flux will linearly decrease the energy splitting between $|L\rangle$ and $|R\rangle$ until it reaches zero at $\Phi_x = \Phi_0/2$. After this crossing the energy splitting flips signs and $|R\rangle$ becomes the lower energy state. Thus we can write the following Hamiltonian for the system:

$$H = \frac{1}{2}\varepsilon\sigma_z\,, \tag{3.18}$$

where we have ε as in Eq. (3.14). Plotted versus applied flux, the two energy eigenstates are linear and cross one another at an applied flux of half a flux quantum, creating a degeneracy in the energy levels (see Fig. 3.5).

This description is actually incomplete if we consider what happens near the degeneracy point. When the double well is close to being symmetric about $\Phi_0/2$, the energy levels in each well can align such that resonant quantum tunneling occurs between wells [58]. This tunnel splitting manifests itself as a

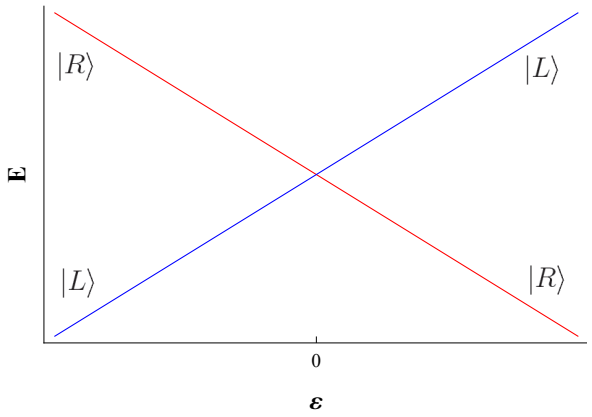

Figure 3.5: Energies of the flux states in the left and right wells as a function of ε in the absence of tunneling, with the degeneracy shown at $\varepsilon = 0$ ($\Phi_x = \Phi_0/2$).

coupling term, Δ, in the system Hamiltonian:

$$H = \frac{1}{2}\left(\varepsilon\sigma_z + \Delta\sigma_x\right) . \tag{3.19}$$

We now turn to the task of obtaining the stationary solutions for this two-level problem, following the methodology of Orlando [59].

From the law of superposition discussed in Section 2.1.1, we can write a state within our two-level in terms of basis states $|L\rangle$ and $|R\rangle$ (note this state could be written in terms of *any* states that form a complete basis):

$$|\psi\rangle\,(t) = c_1(t)\,|L\rangle + c_2(t)\,|R\rangle\ . \tag{3.20}$$

Recalling the form of the Pauli matrices from Section 2.2.1, we write Schrödinger's

equation for the Hamiltonian in Eq. (3.19) as

$$i\hbar \begin{pmatrix} \dot{c_1} \\ \dot{c_2} \end{pmatrix} = \frac{1}{2} \begin{pmatrix} \varepsilon & \Delta \\ \Delta & -\varepsilon \end{pmatrix} \begin{pmatrix} c1 \\ c2 \end{pmatrix} , \tag{3.21}$$

where the overdot is Newton's notation for differentiation with respect to time. To find the desired stationary solutions, we can break up Eq. (3.21) into time-dependent and -independent parts, the former to give the form of the eigenfunctions and the latter to yield the energies and coefficients. Writing the eigenvalue equation, we have

$$\frac{1}{2} \begin{pmatrix} \varepsilon & \Delta \\ \Delta & -\varepsilon \end{pmatrix} \begin{pmatrix} c_1 \\ c_2 \end{pmatrix} = E \begin{pmatrix} c_1 \\ c_2 \end{pmatrix} . \tag{3.22}$$

From this equation and the appropriate determinant we can find the characteristic polynomial and solve for the energies:

$$E_- = -\frac{1}{2}\sqrt{\varepsilon^2 + \Delta^2} \tag{3.23}$$

$$E_+ = \frac{1}{2}\sqrt{\varepsilon^2 + \Delta^2} . \tag{3.24}$$

Note that these expressions for the energies would be more complicated if we did not have the nice feature $H_{11} = -H_{22}$. Looking at these eigen-energies, we can reformulate the energy picture we worked out above. As we approach an external applied flux of $\Phi_0/2$, ε goes to 0. Thus the energy difference $(E_+ - E_-)$ is now Δ rather than 0. The two energies do not cross, resulting in an anticrossing: the tunnel splitting *lifts* the degeneracy that used to be

there. This anticrossing will be of the utmost importance when we discuss Landau-Zener transitions.

To get at the actual wavefunctions, we need to find expressions for the coefficients $c_1^{\pm}$ and $c_2^{\pm}$. After plugging back in our expressions for $E_{\pm}$ and manipulating the matrices, we can define an angle θ in terms of ε and Δ:

$$\sin 2\theta = -\frac{\Delta}{\sqrt{\varepsilon^2 + \Delta^2}} \text{ and } \cos 2\theta = -\frac{\varepsilon}{\sqrt{\varepsilon^2 + \Delta^2}}\,. \tag{3.25}$$

Using the double-angle formulas for sine and cosine, some elementary algebra yields the simple expressions

$$\begin{pmatrix} c_1^- \\ c_2^- \end{pmatrix} = \begin{pmatrix} \cos\theta \\ \sin\theta \end{pmatrix} \text{ and } \begin{pmatrix} c_1^+ \\ c_2^+ \end{pmatrix} = \begin{pmatrix} -\sin\theta \\ \cos\theta \end{pmatrix}\,. \tag{3.26}$$

Recasting the coefficients this way allows us to write the eigenstates in a very compact form. Combining these results with Eq. (3.20), we write the eigenstates as linear combinations of the two flux states $|L\rangle$ and $|R\rangle$:

$$|\psi_-\rangle = \cos\theta\,|L\rangle + \sin\theta\,|R\rangle \tag{3.27}$$

and

$$|\psi_+\rangle = -\sin\theta\,|L\rangle + \cos\theta\,|R\rangle\,. \tag{3.28}$$

These expressions for the eigenstates very quickly tell us what happens at the anticrossing, where the wells are symmetric. The relation $\varepsilon = 0$ together

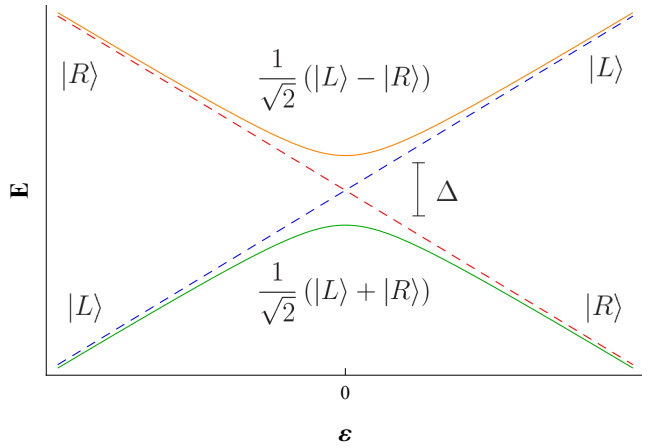

Figure 3.6: Energy diagram of two-level system of flux states, showing both the lifting of the degeneracy and the superposition of states at the anticrossing. Far away from the anticrossing the eigenstates are approximately equal to the basis states.

with Eq. (3.25) imply that the trigonometric functions reduce to $\cos\theta = 1/\sqrt{2}$ and $\sin\theta = 1/\sqrt{2}$. The two eigenstates, then, are equal superpositions of the flux states, with the ground state being symmetric and the excited state antisymmetric (see Fig. 3.6). Hence we have derived the result that Friedman *et al.* and van der Wal *et al.* observed experimentally in 2000. That the flux states of a SQUID can be put into coherent superpositions (thus exhibiting one of the key features of a true quantum two-level system) makes the SQUID a candidate for a qubit.

3.4 Flux Qubits in Practice

While the above analysis illustrates that a SQUID satisfies the requirements to be a qubit, in practice single-junction rings are rarely used. Such systems require high inductances, leading to large rings that are more susceptible to flux

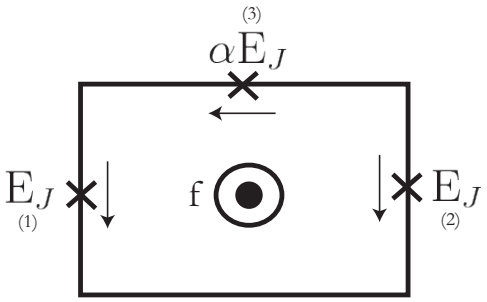

Figure 3.7: Circuit diagram for 3-junction qubit.

noise [6]. We did not mention earlier that though the Stony Brook (Friedman *et al.*) and the Delft (van der Wal *et al.*) groups obtained the same result, they used different systems. The Stony Brook researchers performed their experiments using the rf SQUID outlined above, whereas the Delft group used a three-junction ring proposed by Orlando and Mooij *et al.* [60, 61]. Fig. 3.7 illustrates the new schematic, which has two junctions with identical Josephson energy E_J and a third junction with energy αE_J $(0.5 < \alpha < 1)$.[2] Because of the additional junctions in this circuit, there are now three gauge-invariant phase differences, one across each of the junctions. We assume, however, that the loop is small in this circuit so that we can neglect the inductance of the loop, and thus only the external flux contributes to the total flux. As a result, we can elimnate the gauge-invariant phase of the α-dependent junction by making use of the fluxoid quantization condition: $\varphi_1 - \varphi_2 + \varphi_3 = -2\pi f$, where f is the magnetic frustration (equivalent to ϕ in Section 3.2). The sign of each phase is determined by the direction of current flow through each junction, as

[2]More recently a fourth junction has been added in parallel to this third, α-dependent junction [62]. An independently controlled flux through the resulting loop allowed the group to tune α and hence the energy splitting.

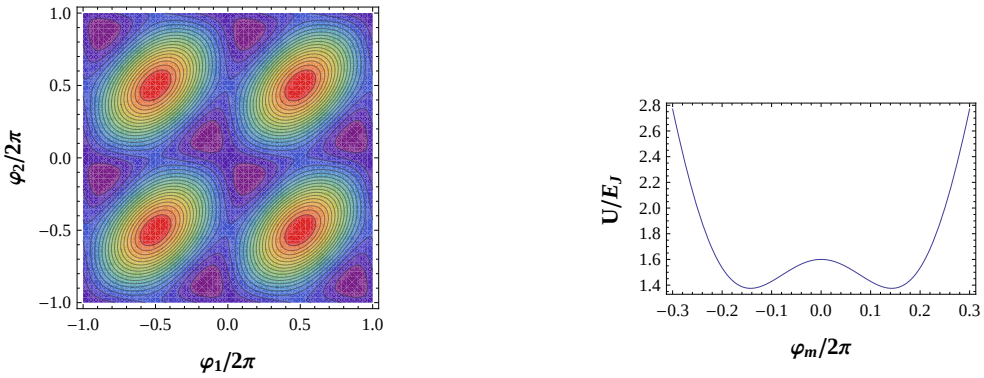

(a) (b)

Figure 3.8: (a) A contour plot of the 3-junction qubit potential with $\alpha = 0.8$ and $f = 0.5$. (b) A slice through one of the figure-eight regions, showing the symmetric, double-well structure.

displayed in Fig. 3.7. The resulting potential of the system is [60]

$$\frac{U}{E_J} = 2 + \alpha - \cos\varphi_1 - \cos\varphi_2 - \alpha\cos(2\pi f + \varphi_1 - \varphi_2)\,, \tag{3.29}$$

where φ_i $(i = 1, 2)$ are the gauge-invariant phase differences. The potential is now a function of two phase variables as illustrated in the contour plot in Fig. 3.8. Near values of $f = 1/2$ and α in the range specified above, the potential forms double wells in the purple, figure-eight-like areas of the plot. Therefore even in this more complicated scheme we are able to recover the desired two-level system. The smaller size of these circuits decreases the amount of coupling to the environment, making the the qubit less sensitive to flux noise. The authors also demonstrated at this early stage that the qubit could be precisely controlled by magnetic fields and could be coupled to other qubits to carry out 2-qubit operations [61]. As a result, this design has become one of the standard implementations of flux qubits.

Chapter 4

Landau-Zener Transitions

In the last chapter we outlined how a superconducting system can exhibit an avoided crossing between flux states. In this chapter we develop, in some detail, one of the useful phenomena that occurs within this kind of energy structure: Landau-Zener (LZ) transitions. These nonadiabatic processes form the basis of our search for a new factorization scheme.

4.1 The Landau-Zener Problem

In 1932, Landau [7], Zener [8], and Stückelberg [9] each derived the probability that a system would make a transition between energy states that did not cross. To arrive at a solution, Zener massaged the differential equations into a form known as Weber's equation, which has parabolic cylinder functions as its solutions.[1] His scheme is rather convoluted, so we will set the context of

[1]More recently, Wittig solved the same problem by taking advantage of the elegance of complex analysis, using contour integrals and the residue calculus [63]. His solution is simpler than Zener's, but I have some misgivings about some of the steps he took so I will

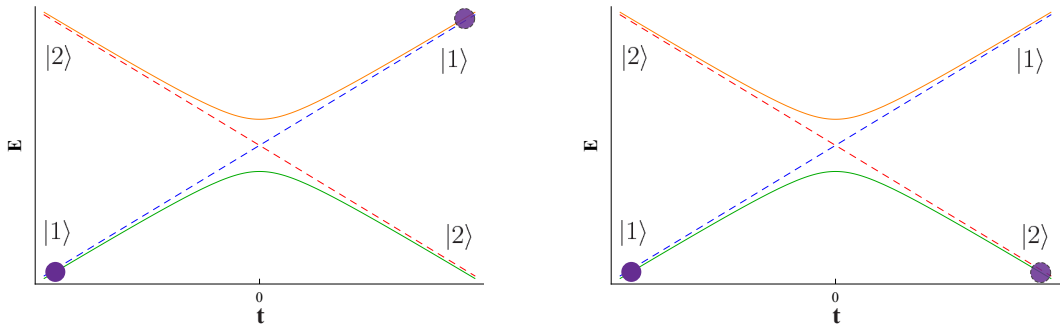

Figure 4.1: The particle (solid purple dot) begins in the lower energy state ($|1\rangle$) at $t = -\infty$. After it passes through the anticrossing it can either end up in the excited state (a) or the ground state (b) by either undergoing a transition or not, respectively.

the problem and give an outline of the method, directing the reader to the original paper for many of the gritty details.

We set up the problem as follows. Given a two-level system whose states have energy levels that exhibit an avoided crossing, if we start in the lower energy state at $t = -\infty$, what is the probability that the system will be in the excited state at $t = \infty$ after we sweep through the anticrossing? Because of the avoided crossing, ending up in the initial uncoupled state (a flux state, for instance) requires that the system undergo a transition across the energy splitting (see Fig. 4.1).[2] Looking at the problem, we can guess that the probability for this transition to occur will be dependent upon the energy splitting, Δ, and the rate at which we sweep through the avoided crossing. The qualitative dependence on the energy splitting is fairly obvious: a larger

stick to a rough sketch of Zener's method.

[2]This actually depends on our basis - if we use the energy eigenbasis, staying in that same state after passing the avoided crossing actually requires that there *not* be a transition. This will become clearer as the chapter progresses.

splitting will decrease the probability of making the transition. The second parameter's role arises from the adiabatic theorem, which states that if we evolve a system slowly enough, then system will remain in the ground state of the new Hamiltonian. Thus if we sweep slowly through the anticrossing, we expect the probability of making the so-called *nonadiabatic* transition to the higher energy level to be small; the system will simply follow the lower eigenenergy. Given this framework, we refer to the energy eigenstates as being in the adiabatic basis and the uncoupled states as being in the diabatic basis.

To simplify the problem, Zener assumed that the energy difference was linear in time. This makes the calculations more tractable, but we will see later that this restriction is not that limiting: even nonlinear scenarios can be well-approximated by the solution presented here. He also assumed that the off-diagonal coupling term and the diabatic basis states were independent of time.

As in Section 3.3, we write the system's state $|\psi\rangle$ as a linear combination of the diabatic basis states $|\phi_1\rangle$ and $|\phi_2\rangle$:

$$|\psi(t)\rangle = A \exp\left[i \int E_1 dt\right] |\phi_1\rangle + B \exp\left[i \int E_2 dt\right] |\phi_2\rangle \ , \tag{4.1}$$

where A and B are time-dependent, complex-valued coefficients and the exponential factors are dynamical phases (where we have set $\hbar = 1$). Assuming the initial condition $|\psi(t = -\infty)\rangle = |\phi_2\rangle$ (we can start in either state, but I am following Zener's convention), our task is to find $|B_f|^2 \equiv |B(t = \infty)|^2$, the probability of being in the excited state after all evolution is complete. This

is equivalent to finding $1 - |A_f|^2$, which is how we will approach the problem.

The matrix for this two-level system is identical to that in Eq. (3.19), except we replace ϵ with the time dependent factor vt so that the energy splitting is linear in time and use Δ instead of $\Delta/2$ (a convention followed by many authors):

$$H(t) = \begin{pmatrix} \frac{vt}{2} & \Delta \\ \Delta & -\frac{vt}{2} \end{pmatrix} . \tag{4.2}$$

From the Schrödinger equation,

$$i\frac{d}{dt}\left|\psi(t)\right\rangle = H(t)\left|\psi(t)\right\rangle , \tag{4.3}$$

we obtain coupled differential equations:

$$\dot{A} = i\,\Delta B \exp\left[-i\int E_{12}dt\right] \tag{4.4}$$

and

$$\dot{B} = i\,\Delta A \exp\left[i\int E_{12}dt\right] , \tag{4.5}$$

where $E_{12} = E_1 - E_2 = vt$ is the energy difference between levels. We can eliminate B by writing $B = \dfrac{\dot{A}}{i\,\Delta \exp\left[i\int vt\,dt\right]}$ and plugging it into Eq. (4.5). After carrying out all the derivatives and combining like terms we obtain

$$\ddot{A} + i\,vt\dot{A} + \Delta^2 A = 0\,. \tag{4.6}$$

The substitutions $A = \exp\left[-i \int vt\, dt\right] U$, $z = \sqrt{v} \exp\left[-i\pi/4\right] t$, and $n = i\,\Delta^2/v = i\,\delta$ (after some tedious algebra) transform Eq. (4.6) into

$$\ddot{U} + \left(n + \frac{1}{2} - \frac{z^2}{4}\right) U = 0\,. \tag{4.7}$$

This is known as Weber's equation, and admits solutions that are parabolic cylinder functions, $D_n(z)$ [64]. The asymptotic forms of these functions yield the following result for $|A_f|^2$:

$$\begin{aligned} |A_f|^2 &= \frac{2\pi\delta e^{-\pi\delta}}{\Gamma(i\delta+1)\Gamma(-i\delta+1)} \\ &= 2e^{-\pi\delta} \sinh \pi\delta \\ &= 1 - e^{-2\pi\delta}\,, \end{aligned} \tag{4.8}$$

where Γ is the Gamma function. Thus the final nonadiabatic transition probability is

$$P_{LZ} = 1 - |A_f|^2 = e^{-2\pi\Delta^2/v}\,. \tag{4.9}$$

Fig. 4.2 illustrates the probability that a particle in state $|1\rangle$ will end up in state $|2\rangle$ after passing through the anticrossing (i.e. this probability is $1-P_{LZ}$). Note that as Δ^2/v increases (so the sweep is more *adiabatic*), the probability of switching states also increases. The Landau-Zener formula provides great agreement with the exact numerics.

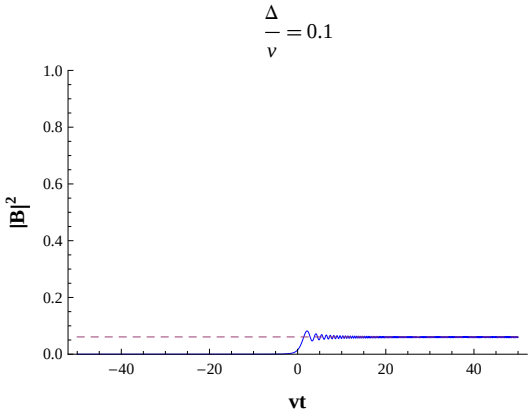

(a)

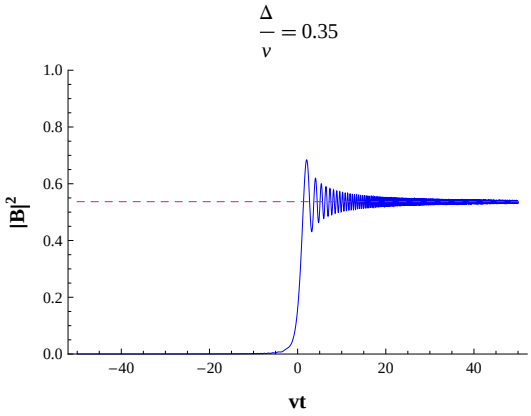

(b)

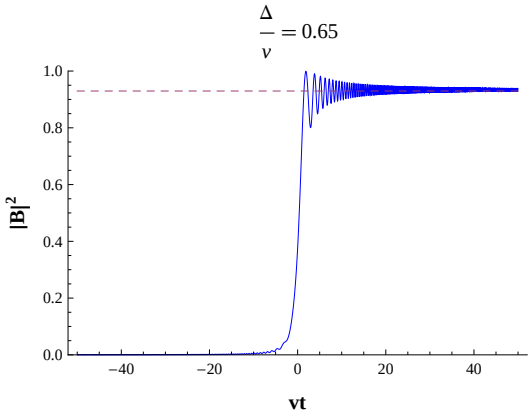

(c)

Figure 4.2: Plots of the probability for the transition $|1\rangle \rightarrow |2\rangle$ to take place for different values of Δ/v. The solid curves are numerical calculations, and the dashed lines are the asymptotic values given by $1 - P_{LZ}$.

4.2 Repeated LZ Transitions

Over the last few years, there has been renewed interest in problems involving LZ transitions that have far richer dynamics. Much attention has been paid to the idea of *repeated* LZ transitions, where one induces many sequential trasitions by driving the system back and forth across the avoided crossing. We explore this problem in the present section by looking at it in various limiting cases. One purpose of this section is to develop an analytical expression for the switching probability as a function of transition number. The other is the resulting quantum inferterence of paths. This forms the foundation for our proposal for an integer factorization scheme, as the condition for constructive interference will determine whether or not an integer is a factor of another number.

4.2.1 Limit of Rapid Oscillations: Coherent Destruction of Tunneling

Before looking at the problem through the lens of LZ transitions, we first present an old result that will provide us with a useful limit to which we can compare the LZ formula. We seek to find the probability that a two-level system under the influence of a harmonic drive will occupy the excited state as a function of time. The system Hamiltonian is identical to the one discussed earlier but with a change in the σ_z term:

$$H = \frac{1}{2} A \cos(\omega t)\, \sigma_z + \Delta\, \sigma_x \,. \tag{4.10}$$

To simplify matters, we will consider the problem in the limit of rapid oscillations, i.e. $\Delta \ll \omega$. First obtained by Grossman and Hänggi [65], Kayanuma also presented the solution in a much clearer form that avoided the abstract Floquet formalism [11]. We follow his presentation in this section.

It is useful to work in the interaction picture (see Appendix B), which results in a state vector of the form

$$|\psi(t)\rangle = c_1(t) \exp\left[-i \int_0^t \frac{A}{2} cos(\omega t')dt'\right] |1\rangle + c_2(t) \exp\left[i \int_0^t \frac{A}{2} cos(\omega t')dt'\right] |2\rangle \ , \tag{4.11}$$

where we have relabeled the basis states $|\phi_i\rangle$ as $|i\rangle$ to simplify the notation. Inserting this state and the Hamiltonian into Schrödinger's equation yields the coupled differential equations

$$i\frac{d}{dt}c_1 = \Delta \exp\left[i\frac{A}{\omega}\sin(\omega t)\right] c_2 \tag{4.12}$$

and

$$i\frac{d}{dt}c_2 = \Delta \exp\left[-i\frac{A}{\omega}\sin(\omega t)\right] c_1 \, . \tag{4.13}$$

The probability of being in the excited state, denoted $P(t)$, is given by $|c_2|^2$.

To exploit the limit $\Delta \ll \omega$, we first make use of the Jacobi-Anger expansion:

$$e^{i\,z\sin\gamma} = \sum_{n=-\infty}^{\infty} e^{i\,n\gamma} J_n(z) \, ,$$

where J_n is the n^{th}-order Bessel function of the first kind. This is a suggestive

equation given the presence of sine functions in the exponential terms of the state vector. Indeed, relating this expression to our problem we obtain

$$\Delta e^{i\,\frac{A}{\omega}\sin(\omega t)} = \Delta \sum_{n=-\infty}^{\infty} e^{i\,n\omega t} J_n(A/\omega). \tag{4.14}$$

Because the oscillations are so rapid in comparison to the energy splitting, the oscillating terms of the sum have a negligible contribution to the population dynamics and only the $n = 0$ term is relevant. Garraway and Vitanov [16] call this the second rotating wave approximation, which yields a nicer equation to solve:

$$e^{i\,\frac{A}{\omega}\sin(\omega t)} \approx J_0(A/\omega)\,. \tag{4.15}$$

We can substitute this back into the coupled differential equations Eqs. (4.12) and (4.13) so that their solution becomes much easier. The straightforward solution of these dynamical equations results in an excited state population of

$$P(t) \approx \sin^2\left[J_0(A/\omega)\Delta t\right]\,. \tag{4.16}$$

Thus in the rapidly oscillating regime, $P_{LZ} \longrightarrow 1$ when A/ω is a zero of the zeroth-order Bessel function, so that there is no tunneling between wells (i.e. the transition $|1\rangle \longrightarrow |2\rangle$ is quenched). This process is often called *coherent destruction of tunneling*. The effect is clearly demonstrated in numerical simulations (see Fig. 4.3), as is the requirement that the coupling be small. Increasing Δ/ω from 0.1 to a value on the order of unity erases the coherent destruction of tunneling, and Eq. (4.16) is therefore invalid. Though it

works in the proper limit, this derivation does not get at the heart of *why* such interference phenomena arise in harmonically driven two-level systems. By considering the process as a series of discrete LZ transition events, Kayanuma elucidates this mystery.

4.2.2 Discretizing the Problem

Though the driving flux is a continous function of time, we can break up one period of a sweep into independent processes, each of which has its own associated matrix. Known as the transfer (or scattering or evolution) matrix method, it has been studied extensively [10–14, 18–20, 66–68]. In this and the following sections we tie these papers together and fill in some of the omitted steps.

We divide up the components of a LZ transition as follows (see Fig. 4.4):

1. Starting completely in the ground state far away from the anticrossing, the system is moved with speed $A\omega \sin(\omega t)$ towards the anticrossing. In this region, the state acquires a dynamical phase based on the difference of energy levels, which are sufficiently separated such that no population transfer between states occurs.

2. The system then passes through the avoided crossing with linear speed $A\omega$, resulting in a superposition of basis states due to a nonadiabatic transition happening with probability P_{LZ}. The matrix characterizing this process is the actual transfer matrix, and we calculate it in the next section.

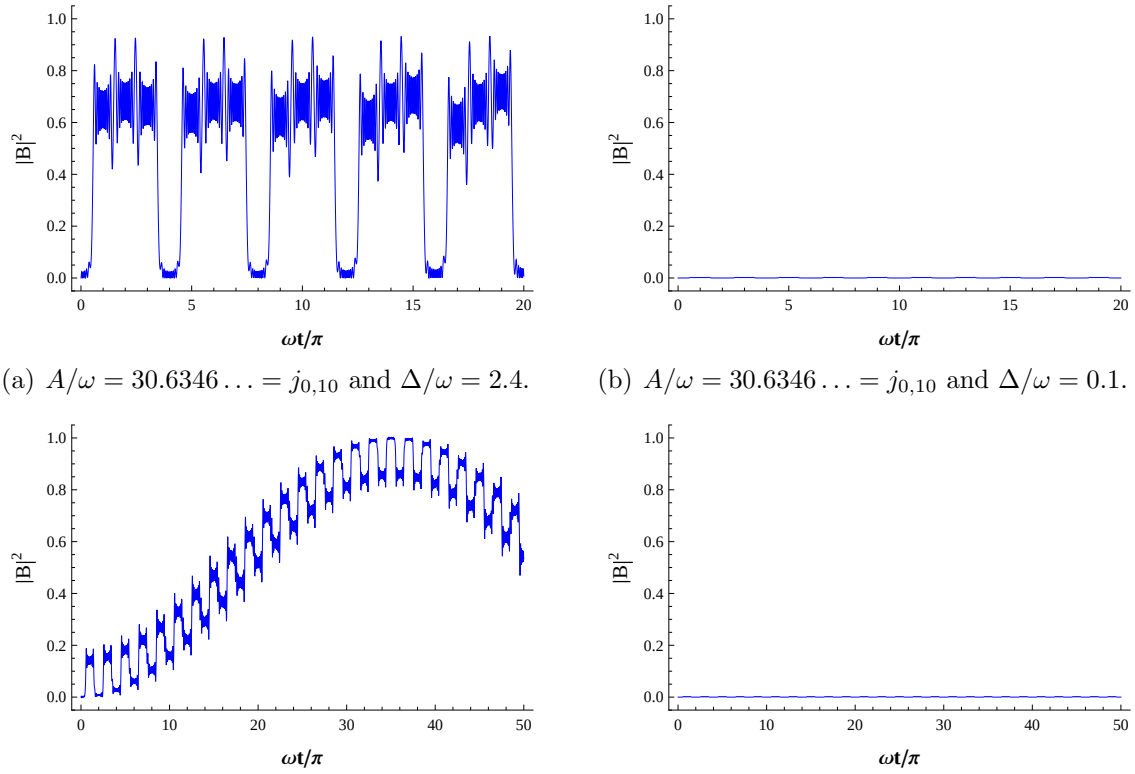

(a) $A/\omega = 30.6346\ldots = j_{0,10}$ and $\Delta/\omega = 2.4$.

(b) $A/\omega = 30.6346\ldots = j_{0,10}$ and $\Delta/\omega = 0.1$.

(c) $A/\omega = 46.3412\ldots = j_{0,15}$ and $\Delta/\omega = 1$.

(d) $A/\omega = 46.3412\ldots = j_{0,15}$ and $\Delta/\omega = 0.1$.

Figure 4.3: Demonstrations of coherent destruction of tunneling for sufficiently small values of Δ and the reemergence of nontrivial population dynamics if the coupling is large (and $j_{n,i}$ is the i^{th} zero of the n^{th}-order Bessel function of the first kind). Also, $|B|^2$ is equivalent to $|c_2|^2$.

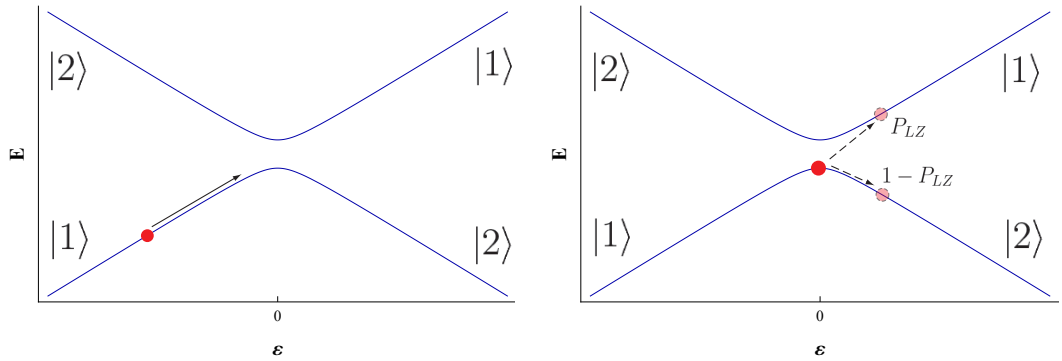

(a) Region 1

(b) Region 2

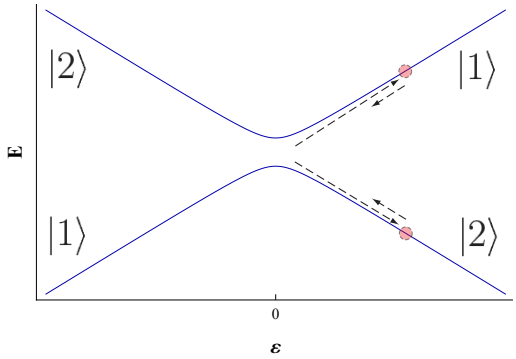

(c) Region 3

Figure 4.4: Different regions of a harmonic Landau-Zener sweep, as outlined in the text.

3. After passing the anticrossing, the state freely evolves and acquires yet more dynamical phase. For convention's sake we will consider the reaching of the turning point to be the completion of one LZ cycle (i.e. $0 \leq t \leq \pi/\omega$ for the first cycle).

In this setup, transitions will occur at times $t_n = (n - 1/2)\pi/\omega$ (with $n \in \mathbb{Z}^+$), since this is where the drive term disappears and the eigenenergies are separated by the flux tunneling, 2Δ. We assume that we are in the limit of strong driving, such that $A \gg \max(\Delta, \omega)$. This ensures that the LZ transition

will happen quickly, since the transition time is estimated to be on the order of $\Delta/A\omega$ or $1/\sqrt{A\omega}$ in the adiabatic ($\Delta^2/A\omega \gg 1$) or diabatic ($\Delta^2/A\omega \ll 1$) limits, respectively [69].

The 2×2 evolution matrix for the dynamical phase possesses a simple form, constructed so that it imparts an exponential phase factor to each of the basis states.[3] The phase is dynamical, hence given by the integral of the energy over the time of evolution:

$$\theta = 2 \int_0^{\pi/2\omega} (E_+ - E_-)\, dt\,, \tag{4.17}$$

where we carry out the integration to the turning point of the drive and multiply the integral by 2 to account for the phase accumulated after the system returns to the avoided crossing (the integral of $\cos(\omega t)$ from 0 to π/ω is 0, but the phase acquired between the anticrossing and the turning point does not cancel the phase acquired on the way back to the anticrossing - the phases add). Recalling the form of the eigenenergies from Section 3.3, $(E_+ - E_-)$ becomes $\sqrt{A^2 \cos^2 \omega t + 4\Delta^2}$. Pulling a factor of A^2 outside the square root and using the limit $A \gg \max(\Delta, \omega)$, the integral evaluates to A/ω. The free evolution is then contained in the following matrix:

$$G_1 = \begin{pmatrix} e^{i\,\theta} & 0 \\ 0 & e^{-i\,\theta} \end{pmatrix}\,, \tag{4.18}$$

[3]Note that we will be conducting all calculations in the *diabatic* basis even though these are not the eigenstates of the Hamiltonian. The eigenstates are very close to the diabatic states far away from the avoided crossing, which is where measurements of flux would be performed in an experiment.

which describes dynamics on the left side of the avoided crossing. On the other side of the anticrossing, the basis states switch energy levels, causing the sign of θ to flip. Thus the dynamical phase acquired to the right of the avoided crossing is $G_2 = G_1^*$.

4.2.3 Calculating the Transfer Matrix

Calculating the transfer matrix proves a far less trivial task than writing down the propagator terms. We want to construct a matrix M_i whose elements $M_{i_{jk}}$ characterize the transition from $|j\rangle$ to $|k\rangle$ as we sweep through the avoided crossing from the right ($i = 1$) or left ($i = 2$). It is the matrix that connects the states immediately before and immediately after the transition. With the LZ probability, P_{LZ}, in hand, we know that $\sqrt{P_{LZ}}$ determines the transition $|j\rangle \rightarrow |j\rangle$ and that $\sqrt{1 - P_{LZ}}$ determines the transition $|j\rangle \rightarrow |k\rangle$, $j \neq k$. Unfortunately, this lacks information about the phase accumulated during the transition. We will sketch the calculation of this phase in order to determine the full transfer matrix.

First, for notational ease, we write $P_{LZ} \equiv q = \exp[-2\pi\delta]$ and $\delta = \Delta^2/(A\omega)$. Recall from Section 4.1 that we were able to manipulate the state vector coefficients into the form of Weber's equation. Yet now we instead take the sweep speed, v, to be $A\omega$ since we assume the transition at the anticrossing to be instantaneous, and $A\omega$ is the value of the derivative of the harmonic drive at that point. We saw earlier that this equation has parabolic cylinder functions as solutions. By looking at the asymptotic forms of these parabolic cylinder functions in different regions of the complex plane, we obtain a phase

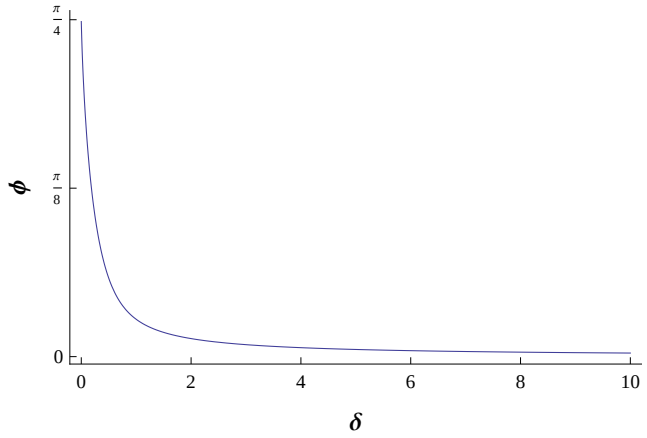

Figure 4.5: Stokes phase as a function of δ.

factor called the Stokes phase (see [14] for full details):

$$\phi = \pi/4 + \delta(\log\delta - 1) + \arg\Gamma(1 - i)\,\delta\,, \tag{4.19}$$

where Γ is the Gamma function. Fig. 4.5 illustrates the Stokes phase's behavior: it approaches $\pi/4$ in the diabatic limit and 0 in the adiabatic limit. It arises only in the off-diagonal terms of the transfer matrix, which are precisely the terms that describe a switch between the diabatic states. Combining this phase and the transition probabilities discussed above with the unitarity condition $M_{21} = -M_{12}^*$, we obtain the full transfer matrix:

$$M_1 = \begin{pmatrix} \sqrt{q} & -\sqrt{1-q}e^{i\,\phi} \\ \sqrt{1-q}e^{-i\phi} & \sqrt{q} \end{pmatrix}. \tag{4.20}$$

If we sweep from the other direction, that transfer matrix, M_2, is just the complex conjugate of Eq. (4.20).

4.2.4 Analytic Expressions

We now possess all the necessary machinery to analytically determine the population of state $|2\rangle$ as a function of LZ transition number. To do this we will determine the full state $|\psi_n\rangle \equiv |\psi(t = n\pi/\omega)\rangle$ and take the square of the modulus of the $|2\rangle$ coefficient. This result was first derived by Kayanuma in [10] and [11], but here we fill in the gaps in his very concise presentation.

We initialize the system in the state $|\psi_0\rangle \equiv \binom{1}{0}$ far away from and on the right side of the anticrossing. As we sweep the flux to the opposite turning point, the system will experience three events: it will accumulate half of the dynamical phase in G_2, undergo an LZ transition, and finally acquire half of the phase in G_1. We can thus write the resultant state vector, $|\psi_1\rangle$, as $G_1^{1/2} M_1 G_2^{1/2} |\psi_0\rangle$. Similarly the next state is given by $|\psi_2\rangle = G_2^{1/2} M_2 G_1^{1/2} |\psi_1\rangle = G_2^{1/2} M_2 G_1 M_1 G_2^{1/2} |\psi_0\rangle$, and so on. Given the repetitive nature of this process, it is helpful to define a new matrix T,

$$T \equiv G_1^{1/2} M_1 G_2^{1/2} = \begin{pmatrix} \sqrt{q} & -\sqrt{1-q} e^{i(\phi+\theta)} \\ \sqrt{1-q} e^{-i(\phi+\theta)} & \sqrt{q} \end{pmatrix} , \tag{4.21}$$

which describes the complete cycle for a single LZ transition. Given how we defined the evolution matrices, T^* represents the same process but in the opposite direction. This will simplify our expressions for the general n^{th} state vector as a result of the following matrix multiplication:

$$T^* T = (G_1^{1/2} M_1 G_2^{1/2})^* (G_1^{1/2} M_1 G_2^{1/2}) = G_2^{1/2} M_2 G_1 M_1 G_2^{1/2} , \tag{4.22}$$

a factor we already see in the expression for $|\psi_2\rangle$. In general, even-numbered states $|\psi_{2m}\rangle$ will see m factors of T^*T and odd-numbered states will see $m-1$ factors of T^*T with an additional T for that final sweep from the right:

$$|\psi_{2m-1}\rangle = T(T^*T)^{m-1}\,|\psi_0\rangle \tag{4.23}$$

and

$$|\psi_{2m}\rangle = (T^*T)^m\,|\psi_0\rangle\ . \tag{4.24}$$

Though not immediately obvious, it is useful to define yet another matrix:

$$S = \begin{pmatrix} \sqrt{1-q}e^{-i\,(\phi+\theta)} & \sqrt{q} \\ -\sqrt{q} & \sqrt{1-q}e^{i\,(\phi+\theta)} \end{pmatrix}\ . \tag{4.25}$$

After some tedious algebra, we obtain two useful relations:

$$T^*T = -S^2 \tag{4.26}$$

and

$$S^2 = 2\cos\xi\, S - 1\,, \tag{4.27}$$

where we define ξ by $\cos\xi \equiv \sqrt{1-q}\cos(\phi+\theta)$. These equivalences will allow us to derive a recursion relation that generates a closed-form expression for the general state after n transitions.

We consider the equation in Eq. (4.27) to be the $n = 2$ case of a more general relationship: $S^n = \alpha_n + \beta_n S$ where we have $\alpha_2 = -1$ and $\beta_2 = 2\cos\xi$. Similarly for the $n = 1$ case, β_1 equals 1 whereas α_1 is 0. The trivial case of $n = 0$ yields $\beta_0 = 0$. Upon inspecting these three cases, we note that $\alpha_1 = 0 = \beta_0$ and $\alpha_2 = -1 = -\beta_1$. These suggest that the recurrence relation $\alpha_{n+1} = -\beta_n$ between the α's and the β's. Indeed this relationship between α and β is necessary if we want to obtain a recurrence relation for β_n, since we need a way to eliminate any α.

To calculate the recursion for β_n, we first start with the expression for S^n but replace the α_n with $-\beta_{n-1}$:

$$S^n - \beta_n S + \beta_{n-1} = 0\,.$$

This implies

$$0 = S(S^{n-1} - \beta_n) + \beta_{n-1} = S(\underbrace{-\beta_{n-2}}_{\alpha_{n-1}} + \beta_{n-1}S - \beta_n) + \beta_{n-1}\,.$$

By regrouping terms by powers of S and using Eq. (4.27), we arrive at

$$S\left(-\beta_{n-2} - \beta_n + 2\cos\xi\,\beta_{n-1}\right) = 0.$$

S is a nontrivial matrix, thus the terms within the parentheses sum to 0. Reindexing the β's and multiplying by -1, we finally obtain

$$\beta_{n+1} - 2\cos\xi\,\beta_n + \beta_{n-1} = 0\,, \tag{4.28}$$

the recurrence relation for β.

To find β_n, we write the characteristic polynomial of Eq. (4.28):

$$x^{n+1} - 2\cos\xi\, x^n + x^{n-1} = x^{n-1}(x^2 - 2\cos\xi\, x + 1) = 0.$$

Solving for x via the quadratic formula yields $x = e^{\pm i\,\xi}$, so the full solution is of the form $ae^{i\,n\xi} + be^{-i\,n\xi} = \beta_n$. The initial conditions $\beta_0 = 0$ and $\beta_1 = 1$ imply that $a = -b$ and $a = \frac{1}{2i\,\sin\xi}$. Therefore we have

$$\beta_n = \frac{1}{2i\,\sin\xi}\left(e^{i\,n\xi} - e^{-i\,n\xi}\right) = \frac{\sin n\xi}{\sin\xi}\,, \tag{4.29}$$

a compact expression for β_n.

All that remains is to calculate the actual states as a function of LZ transition number. For the odd case, we have the following string of equalities:

$$\begin{aligned}
|\psi_{2m-1}\rangle &= T(T^*T)^{m-1}\,|\psi_0\rangle \\
&= T(-1)^{m-1}S^{2m-2}\,|\psi_0\rangle \\
&= (-1)^{m-1}T(\beta_{2m-3} + \beta_{2m-2}S)\tbinom{1}{0} \\
&\;\;\vdots \\
&= (-1)^{m-1}\begin{pmatrix} \beta_{2m-1}\sqrt{q} \\ \beta_{2m-1}\sqrt{1-q}e^{-i\,(\phi+\theta)} - \beta_{2m-2} \end{pmatrix},
\end{aligned} \tag{4.30}$$

where we have omitted some of the intermediate steps since they involve elementary but tedious matrix manipulations. Finding $|\psi_{2m}\rangle$ is similar and actually easier due to the lack of an extra factor of T, with the final result

being

$$|\psi_{2m}\rangle = (-1)^m \begin{pmatrix} \sqrt{1-q}e^{-i(\phi+\theta)}\beta_{2m} - \beta_{2m-1} \\ -\sqrt{q}\beta_{2m} \end{pmatrix}. \tag{4.31}$$

Finally, we can take the square of the modulus of the $|2\rangle$ coefficient to obtain the analytical expressions for the probability of being in the excited state after n transitions:

$$P_{2m-1} = 1 - q\left[\frac{\sin[(2m-1)\xi]}{\sin\xi}\right]^2 \tag{4.32}$$

and

$$P_{2m} = q\left[\frac{\sin(2m\xi)}{\sin\xi}\right]^2. \tag{4.33}$$

These simple formulas do a remarkable job of calculating the corrcect probability of occupying $|2\rangle$ over a wide range in parameter space, as the simulations in Fig. 4.6 illustrate.

If we take the diabatic limit, $\delta \ll 1$, then we can recover the time-dependent probability obtained in Section 4.2.1. This limit implies the following values for our parameters: $q \to 1$, $\phi \to \pi/4$, and $\theta \to A/\omega$ [11]. Thus we have $q = e^{-2\pi\delta} \approx 1 - 2\pi\delta$. Because q approaches 1, $\cos\xi$ goes to 0, hence $\sin\xi \to 1$. Therefore the probabilities in Eqs. (4.32) and (4.33) become

$$P_{2m-1} \approx 1 - [\sin[(2m-1)\xi]]^2 = \cos^2[(2m-1)\xi] \tag{4.34}$$

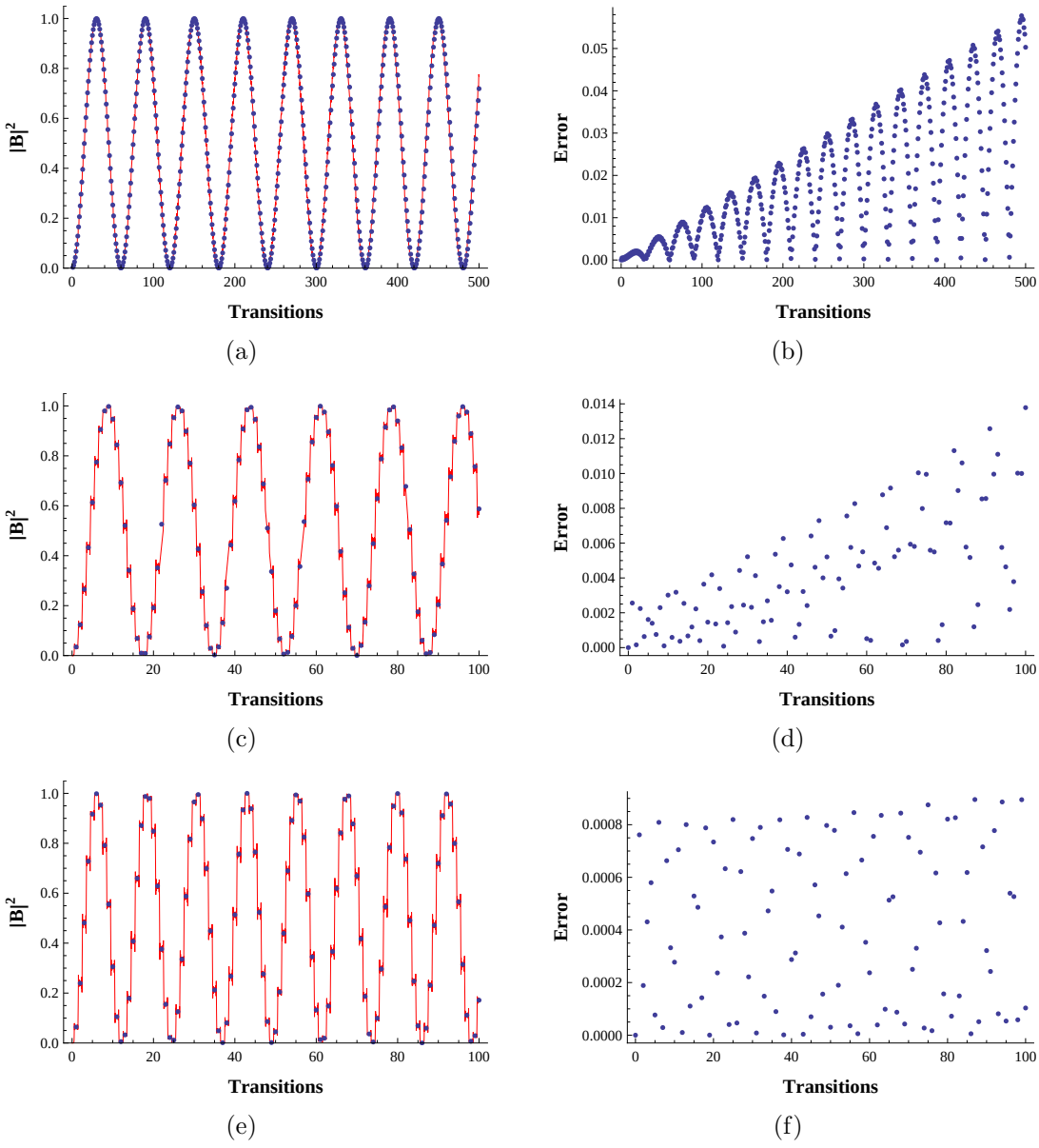

Figure 4.6: Comparison of Eqs. (4.32) and (4.33) (blue dots) with the numerical integration of the Hamiltonian (red lines) for (a) $A/\omega = 20$ and $\Delta/\omega = 0.1$, (c) $A/\omega = 45$ and $\Delta/\omega = 0.5$, and (e) $A/\omega = 95$ and $\Delta/\omega = 1$. Figures (b), (d), and (f) show the respective errors between the equations and the numerics for each case.

and

$$P_{2m} \approx \sin^2(2m\xi)\,. \tag{4.35}$$

Noting that in this limit $\pi/2 - \xi$ is small, we have

$$\pi/2 - \xi \approx \sin(\pi/2 - \xi) = \cos\xi \approx \sqrt{2\pi\delta}\sin\left(A/\omega + \pi/4\right)\,,$$

where we have inserted the limiting values of the three parameters q, ϕ, and θ. We solve this equation for ξ and insert that value into the approximate expressions for P_{2m} and P_{2m-1}. This allows us to group both the odd and even terms together with the final result being

$$P_n = \sin^2\left[n\Delta\sqrt{\frac{2\pi}{A\omega}}\sin\left(\frac{A}{\omega} + \frac{\pi}{4}\right)\right]\,. \tag{4.36}$$

Calculating probabilities from this formula is much less computationally taxing than using the full analytical results given in Eqs. (4.32) and (4.33). We can see from the simulations that it follows the exact numerics quite nicely in the diabatic limit (see Fig. 4.7). It also agrees with Eq. (4.16) if we note the asymptotic form of $J_0(x)$ when x is large: $J_0(x) \backsimeq \sqrt{2/\pi x}\sin[x + \pi/4]$ (see, e.g., [64]), where, in our case, $x = A/\omega$.

This remarkable agreement in various limits is even more startling when we consider that we derived them using Zener's original formulation, which finds the probability based on asymptotic values and assumes that the sweep is linear throughout the whole process. In the repeated transition scenario, the sweep is linear only at the avoided crossings. This suggests that the final

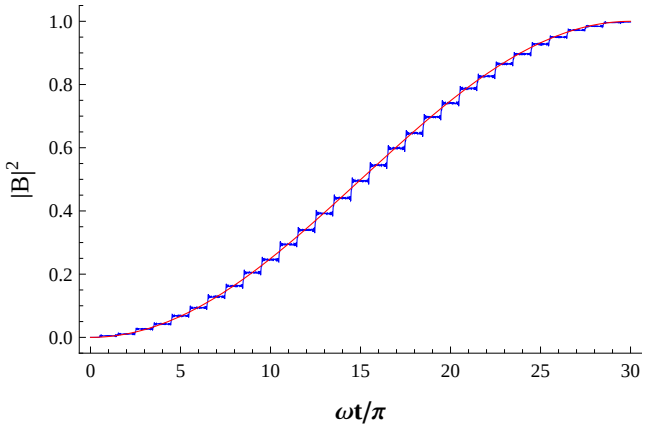

Figure 4.7: Comparison of numerical calculations (blue) with Eq. (4.36) (red) for $A/\omega = 300$ and $\Delta/\omega = 0.5$.

probability of a transition depends more heavily on the dynamics very close to the avoided crossing.

4.3 Landau-Zener Gates

As we have seen, LZ transitions allow us to control both the populations and phases of the two states. Indeed, by appropriately choosing the sweep function or coupling strength we can construct any transition probability between 0 and 1, as demonstrated by Garanin and Schilling [70] and by Wubs *et al.* [67]. The free evolution of the qubit between LZ transitions and the Stokes phase determine the phase of the state. The precise control one can have over this system has inspired physicists to consider LZ transitions as a possible implementation of gate operations in a quantum computer [14, 18, 27, 28, 71] and a means of creating entanglement [29–31].

Using LZ transitions to perform gate operations contrasts the more com-

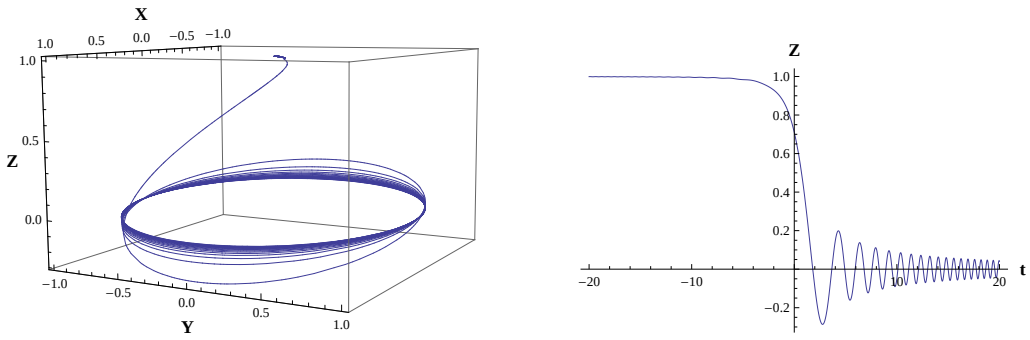

(a) (b)

Figure 4.8: Using an LZ transition to rotate a qubit into the XY plane, with parameters $\Delta = 0.25$ and $v = 0.56$.

mon method involving Rabi oscillations. Typically a qubit is prepared in its ground state far from the anticrossing. We then apply a sharp pulse to bring the system nearer to the anticrossing, where the energy levels are more closely spaced. Here the system undergoes coherent oscillations for a specified amount of time before another pulse brings it back away from the avoided crossing. The oscillation frequency and time of evolution determine the resultant state [14]. The LZ framework, on the other hand, uses smooth pulses that bring the system through the anticrossing, allowing P_{LZ} and phase to induce the final state population.

As an example we consider a tunnel splitting of $\Delta = 0.25$ and a sweep speed of $v = 0.56$. If we solve the problem using the density matrix formalism [72], we can calculate the X, Y, and Z components of the qubit's Bloch sphere representation. Fig. 4.8 illustrates both the full Bloch sphere and the Z-component dynamics of the system. The chosen parameters put the qubit in the XY-plane, and by letting it freely evolve after the LZ transition, we can realize the Hadamard gate, for instance. The jump in Z is rather large given

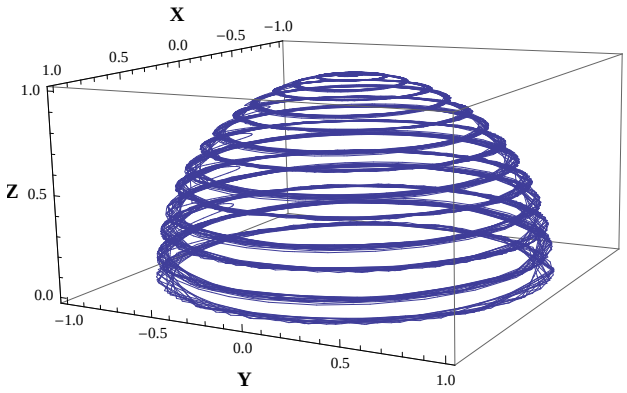

Figure 4.9: Using repeated LZ transitions to rotate a qubit into the XY plane, with parameters $\Delta = 0.04$, $A = 12$, and $\omega = 0.2$.

our choice of Δ and v, and we could instead realize a similar rotation into the XY plane using a series of smaller LZ transitions by harmonically driving the system (see Fig. 4.9 for a rough example).

4.4 Summary

In this chapter we have presented the theory of Landau-Zener transitions in some detail, focusing on the dynamics of a system undergoing repeated transitions. Despite the derivations being rather convoluted, we can succintly summarize the relevant physics. For one sweep, the probability of making a nonadiabatic transition is determined by the sweep speed and the energy splitting of the system in the so-called adiabaticity parameter: Δ^2/v. If we carry out sequential passes through the avoided crossing region of the energy spectrum, however, this parameter does not tell the whole story. Because the

anticrossing acts as a form of a beam splitter and creates a coherent superposition of basis states, the two "paths" of the particle can interfere with one another when they reconverge at the next passing of the anticrossing. As with other interference effects, this is a phase-dependent phenomenon, and in this problem there are two phases at work: the dynamical phase accumulated away from the anticrossing and the Stokes phase associated with the LZ transition. We will see in the next chapter that we can gain precise control of the interference by driving the system off of center so that the phases developed on either side of the avoided crossing are different.

Chapter 5

Factorization

The *fundamental theorem of arithmetic* states that any positive integer $n \in \mathbb{Z}^+$ can be factorized into a unique product (up to the order of the factors) of prime numbers:

$$n = p_1 \times p_2 \cdots \times p_r \,,$$

where each p_i is a - not necessarily distinct - prime. Given a handful of prime numbers, it is straightforward to determine what integer their product yields: simply multiply them together. The inverse procedure, however, proves to be far less trivial and has plagued mathematicians for millenia [73]. To date, no one has proved that factoring large integers is a computationally difficult problem, but the most efficient known classical algorithm still scales only exponentially with input number. Given the extent to which integer factorization has been studied, most computer scientists agree that an efficient factoring algorithm does not exist. Here we take "efficient" to mean that both the running time of and the needed resources for the algorithm will behave as

polynomial functions of the number of bits needed to represent the problem. The inherent difficulty of factoring large integers provides the basis for public-key encryption via RSA.

In 1994 Peter Shor rocked the computer science and physics worlds with his development of a quantum algorithm that could efficiently factor large integers with a quantum computer [4]. While much attention has been devoted to the realization of Shor's algorithm on an actual quantum computer, there has been a recent exploration into other factoring methods based on diffraction [35, 74]. Loosely referred to as Gauss sums (see Appendix C and a wealth of literature: [36, 75–83]), physicists have realized these schemes experimentally, but have yet to demonstrate exponential speedup. By bringing together the material thus far presented in this thesis, we propose a new method based on the interference from repeated Landau-Zener transitions that has the potential for improved efficiency over previous diffraction-based procedures.

In this chapter we will first set the context with a discussion of diffraction-based factoring as proposed by Clauser and Dowling. The bulk of the chapter deals with the details of our method, and we consider scaling laws, physical constraints, and potential speedup via quantum entanglement.

5.1 Factorization and Diffraction

Inspired by Shor, Clauser and Dowling investigated the use of classical interferometry for factoring integers [35]. Relying only on classical wave mechanics, their method did not exploit the properties of quantum mechanics that gave

Shor's algorithm its power. Nevertheless, their result is an interesting one and has inspired an array of factorization schemes, some of which have the potential to exploit quantumness to achieve speedup over classical factorization methods. Much like our proposal, this method is a pure utilization of physical resources rather than an exercise in algorithmic efficiency.

Their system consists of the standard Young's N-slit interferometer. The number of slits is set to the composite number to be factored, which they take to be odd (since any even number can be quickly reduced to an odd number if it is not a power of 2). The test factors are encoded in a discrete set of wavelengths, $\lambda_n = a^2 n/R$, where a is the period of the slits, R is the distance between the diffraction grating and the screen, and n is the (odd) test factor. They found that if n is a factor of N, then the resulting diffracton pattern will have spikes of a constant height, proportional to N^2/n. If n is not a factor, however, this does not hold, and there is an observable variance in the diffraction peaks. Thus by setting up an appropriate N-slit diffraction grating and shining light with a wavelength related to the test factor, they need only look for a constant diffraction pattern to determine if n is a factor for not. The problem with this scheme is that the number of slits scales as N, which is exponential in the number of bits needed to represent N.[1]

A year later in 1997, Summhammer extended the result of Clauser and Dowling to a Mach-Zehnder interferometer [74]. In the next section we explain in detail what a Mach-Zehnder interferometer is, but the take home

[1]The number of bits, b, needed to represent N in binary is roughly equal to $\log N$, where the logarithm is taken base 2. Thus N is given by $N = 2^b$, so a polynomial scaling in N will be exponential in b.

message is that instead of varying parameters like the distance between slits to test a factor, we can adjust the phase shift of the legs of an interferometer. By adjusting the phase shift, χ, in discrete steps of $2\pi/n$, we have the set of phases: $\chi_j = 2\pi j/n$. The idea is to make an observation of one of the detectors at the end of the interferometer whenever $j = kN$, with N, as usual, being the input composite number. As we show below (and using the relation $\cos^2\theta = \frac{1}{2}[1 + \cos 2\theta]$), the probability of the detector observing a particle is $p(k) = \frac{1}{2}\left[1 + \cos\left(\frac{2\pi kN}{n}\right)\right]$. Performing n observations of that detector yields the intensity

$$I_n = \frac{n}{2} + \frac{1}{2}\sum_{k=1}^{n} \cos\left(\frac{2\pi kN}{n}\right) , \tag{5.1}$$

so that if n is a factor of N, the intensity is equal to n as a result of the coherent adding of terms in the sum. But if n is not a factor, the terms of the sum roughly cancel one another since the phases will not all be integer multiples of 2π, resulting in an intensity of $n/2$. Summhammer notes, however, that there are some drawbacks to his scheme as well. The longest possible factor check, for a test factor near $\sqrt{N}$, will be on the order of $N^{3/2}$ so that the problem does not scale well in time. He also outlines a method for using one particle but multiple interferometers to test more than one factor, but the number of interferometers needed scales polynomially with N. So, as with Clauser and Dowling's proposal, no speedup has been achieved.

Despite the shortcomings of these proposals, they provide a novel approach to factoring beyond Shor's and the classical algorithms known to date. By exploiting quantum entanglement, it might be possible to improve upon these early first attempts, which is precisely our goal in the following proposal.

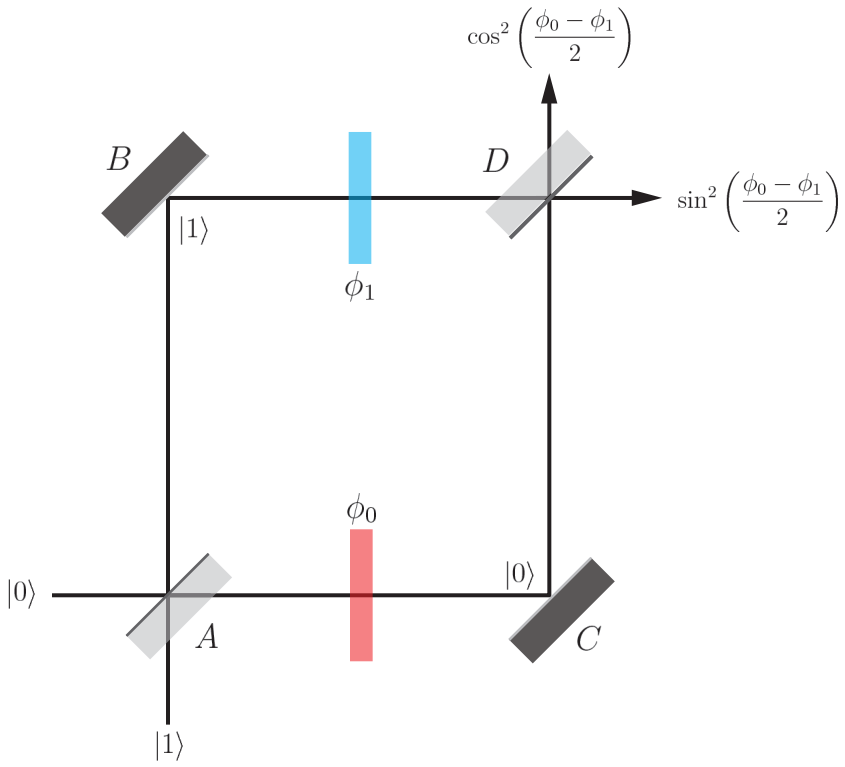

Figure 5.1: A schematic of the Mach-Zehnder interferometer. A and D represent beam splitters, whereas B and C are fully reflecting mirrors.

5.2 Factoring with Repeated LZ Transitions

5.2.1 A Mach-Zehnder Interferometer

Our attempt to factor integers with LZ transitions begins with the Mach-Zehnder interferometer. The schematic in Fig. 5.1 illustrates the basic setup of such a device, where we can imagine the black paths as representing traveling photons. The purpose of this apparatus is to determine the phase difference between the mysterious red and blue materials (or, even more simply, a difference in lengths of the two associated arms). While this setup is normally

realized with beams of light traveling through optics and interfering with one another, we instead want to envision a two-level quantum system working its way through the device (seeing as we have been dealing with flux states in SQUIDS and not light beams, this seems reasonable). Suppose we begin in the path designated $|0\rangle$ in the diagram, by which we mean the system is prepared in the state $|0\rangle$. This state first encounters a beam splitter at A, which creates equal probability amplitudes of the state heading towards mirrors C and B. Along each path the state acquires phases ϕ_0 and ϕ_1 before the two possible paths interfere at the second beam splitter, D. Given the setup, the probabilities of the photon reaching either detector at the end encode the phase information of the system, and these probabilities are easily calculated using some of the simple machinery developed in Chapter 2 (and following the discussion in [41]):

$$\begin{aligned}
|0\rangle &\xrightarrow{H_A} \frac{1}{\sqrt{2}}(|0\rangle + |1\rangle) \\
&\xrightarrow{\phi_0,\,\phi_1} \frac{1}{\sqrt{2}}\left(e^{i\,\phi_0}\,|0\rangle + e^{i\,\phi_1}\,|1\rangle\right) = \frac{e^{i\,(\phi_0+\phi_1)/2}}{\sqrt{2}}\left(e^{i\,(\phi_0-\phi_1)/2}\,|0\rangle + e^{i\,(-\phi_0+\phi_1)/2}\,|1\rangle\right) \\
&\xrightarrow{H_D} e^{i\,(\phi_0+\phi_1)}\left(\cos\left[(\phi_0-\phi_1)/2\right]|0\rangle + i\,\sin\left[(\phi_0-\phi_1)/2\right]|1\rangle\right)\,, \qquad (5.2)
\end{aligned}$$

where we have used the notation H_A, H_D to motivate thinking about beam splitters as Hadamard gates. The last equation gives us the probabilities that we will measure the state to be in either $|0\rangle$ or $|1\rangle$: $\cos^2\left(\frac{\phi_0-\phi_1}{2}\right)$ or $\sin^2\left(\frac{\phi_0-\phi_1}{2}\right)$, respectively. Thus the resulting interference pattern contains the relevant phase information.

What does this have to do with LZ transitions? In 2003, Shytov *et al.*

proposed using repeated LZ transitions as a means for performing interferometry with superconducting qubits [71]. A year later physicists reported the first LZ transitions in such a system [17], but they explored only single rather than sequential transitions. At the end of 2005 and start of 2006, a group from MIT [21] and a group in Finland [18, 19] observed the first experimental evidence for interference due to multiple LZ transitions in flux qubits and charge qubits, respectively. Since we have dealt with flux qubits thus far, we will direct most of our attention to MIT group's original paper and some of their later results [22–25] (much of the discussion in the Finnish group's work, however, is completely analogous).

Though Shytov *et al.*'s paper first put forth this idea of interferometry via LZ transitions, they worked in the regime of weak drive fields whereas the MIT group dealt with strong driving. We also work in the latter limit, and thus follow the MIT discussion of relating repeated LZ transitions to a Mach-Zehnder interferometer. As we mentioned before, the process involves quantum states of our qubit rather than photons. For our beamsplitter we use the avoided crossing, which creates superpositions of the two qubit states that we can tune via the energy splitting and sweep rate. The dynamical phase resulting from the energy difference (see Fig. 5.2) produces the phase shift like the one seen in Fig. 5.1. The state then comes back to the avoided crossing (the second beam splitter) where it interferes with itself. The process is just like the one illustrated in Fig. 4.4. Whether or not the state ends up in $|R\rangle$ or $|L\rangle$ (since we are back to talking about flux qubits, we will use this notation to refer to the two wells) after the second transition depends on the phase

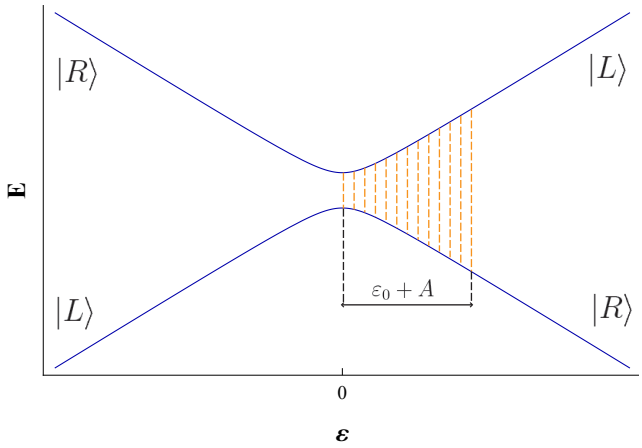

Figure 5.2: The orange region represents the dynamical phase accumulated on the right side of the anticrossing.

acquired between transitions:

$$\Delta\theta_{12} = \frac{1}{\hbar}\int_{t_1}^{t_2}(E_{|R\rangle} - E_{|L\rangle})dt\,, \tag{5.3}$$

where we have re-introduced $\hbar$ for a brief moment to remind the reader that the upcoming equations will deal with multiphoton transitions, hence energy. The interference at the second transition will be constructive if $\Delta\theta_{12}$ is an integer or half-integer multiple of 2π. While this is useful for visualizing LZ transitions as a Mach-Zehnder interferometer, we want to carry out many of these two transition cycles. To do this, the MIT group drove the qubit through the anticrossing with a harmonic signal, but with an added dc flux detuning term, ε_0:

$$\varepsilon(t) = \varepsilon_0 + A\cos(\omega t)\,, \tag{5.4}$$

where we require that $A > \varepsilon$, else no LZ transitions would occur because the

state would never sweep through the anticrossing. With the two transitions, we cared only about the phase accrued on one side of the anticrossing. But now the state will continue to develop phase as it returns to its initial position and the process repeats itself. Thus the relevant quantity is now the phase accumulated over a complete drive cycle. If ε_0 is zero, then the sweeps are symmetric about the anticrossing, and the phase from the right side of the anticrossing will completely cancel the phase from the left. For nonzero values of ε_0, however, the phases will not cancel, as the system will be spending unequal times on either side of the anticrossing. This phase, then, is given by [25]

$$\theta = \frac{1}{\hbar} \oint (E_{|R\rangle} - E_{|L\rangle}) dt = \frac{2\pi\varepsilon_0}{\hbar\omega} \,. \tag{5.5}$$

Thus constructive interference occurs if the condition $\theta = 2\pi n$ is met. In terms of ε_0 this becomes

$$\varepsilon_0 = n\hbar\omega \,. \tag{5.6}$$

This formula suggests that we can view coherent population oscillations (or, equivalently, time-averaged populations of 0.5) as multiphoton transitions, where being on resonance is like absorbing n photons, each with energy $\hbar\omega$. It is this resonance condition that motivates our factoring scheme. If we let ε_0 be our composite number, for instance, then we will get population oscillations only if the energy of the drive is a factor of ε_0. This is similar to the Gauss sum proposal for factorization, where terms in the sum added constructively only if the exponential phase factors were integer multiples of 2π. We explore factorization via this resonance condition in more detail in the following

sections.

5.2.2 The Strong-Driving Limit

In this section we reproduce the analytic result for the switching probability given by the MIT group in [21] and compare it with numerical integration of the Hamiltonian to test its validity. The Hamiltonian is that of a standard two-level system, but we now have a harmonically varying detuning given by Eq. (5.4):

$$H = -\frac{1}{2}\left(\left(\varepsilon_0 + A\cos\omega t\right)\sigma_z + \Delta\,\sigma_x\right)\,. \tag{5.7}$$

We work in the strong driving regime, where the drive and the photon energy are much larger than the energy splitting: $A, \omega \gg \Delta$ (we have reverted back to $\hbar = 1$ for ease of notation, but the reader should by now be aware that ε_0 and A are *energies*, and so all ω's are associated with energies, too). We also want fast LZ transitions to occur so that the probability of staying in the same flux state is near 1. This ensures that any oscillations in excited state population are actually due to constructive inteference with many small transitions adding coherently, rather than a few, isolated transitions with large probabilities occurring. This implies that we operate in the diabatic limit, $\Delta^2/A\omega \ll 1$.

The first step for dealing with this system is to switch to a nonuniformly rotating frame. Defining an angle $\phi(t) = \frac{A}{\omega}\sin(\omega t)$ (the integral of the time-dependent part of $\varepsilon(t)$), we make the transformation:

$$H = e^{-i\,(\phi(t)/2)\sigma_z} H' e^{i\,(\phi(t)/2)\sigma_z}\,, \tag{5.8}$$

where we use the following relation for exponentiated Pauli operators

$$e^{i\,\theta(\hat{n}\cdot\vec{\sigma})} = \cos\theta + i\,(\hat{n}\cdot\vec{\sigma})\sin\theta\,.$$

Carrying out the matrix multiplication, we then have the transformed Hamiltonian [21]:

$$H' = -\frac{1}{2}\begin{pmatrix} \varepsilon_0 & \Delta e^{-i\,\phi(t)} \\ \Delta e^{i\,\phi(t)} & -\varepsilon_0 \end{pmatrix}. \tag{5.9}$$

We can actually isolate each n-photon transition by making use of the Jacob-Anger expansion, $e^{i\,A/\omega\sin(\omega t)} = \sum_{n=-\infty}^{\infty} J_n(A/\omega)e^{-i\,n\omega t}$, which decomposes $\phi(t)$ into its Fourier components. Thus for each resonance there is a new Hamiltonian

$$H_n = -\frac{1}{2}\begin{pmatrix} \varepsilon_0 & \Delta_n e^{-i\,n\omega t} \\ \Delta_n e^{i\,n\omega t} & -\varepsilon_0 \end{pmatrix}, \tag{5.10}$$

where we have defined a photon number-dependent energy splitting $\Delta_n \equiv \Delta J_n(A/\omega)$. This Hamiltonian has a standard solution (see, e.g., Problem 9.20 in [84]). The time-dependent coeffcient for the left well, $c_{|L\rangle}(t)$ (assuming that $c_{|R\rangle}(0) = 1$), is given by

$$c_{|L\rangle}(t) = \frac{i}{\omega'}\Delta_n \sin\left(\frac{\omega' t}{2}\right) e^{-i\,n\omega t}\,, \tag{5.11}$$

where $\omega' = \sqrt{(\varepsilon_0 - n\omega)^2 + |\Delta_n|^2}$. To get the probability we just take the modulus squared of Eq. (5.11). But that gives us information about only one value of n. To know the full switching probability, we must sum over all

possible values of n:

$$P_{SW} = \sum_{n=-\infty}^{\infty} \frac{|\Delta_n|^2}{(\varepsilon_0 - n\omega)^2 + |\Delta_n|^2} \sin^2\left(\frac{\omega' t}{2}\right) . \tag{5.12}$$

Looking at Eq. (5.12), we can glean some qualitative properties at first glance. First, this resembles our earlier result from Mach-Zehnder interferometry in that the final population contains phase information (which is determined by ε_0 in our system). Second, if we ignore the time-dependence for a second, this describes Lorentzian distributions of width $|\Delta_n|$ about the n-photon resonances. Third, if A/ω is a zero of a Bessel function, coherent destruction of tunneling again occurs, and the switching probability drops to zero.

Often we measure time-averaged populations to get information about the system, in which case the $\sin^2\left(\frac{\omega' t}{2}\right)$ term becomes 1/2. The time-averaged solution is given as a density plot in Fig. 5.3. We see from the plot that our qualitative assessment of P_{SW} is correct: resonances occur at integer multiples of ε_0/ω, and there are lobes along the A/ω axis determined by zeros of Bessel functions. The figure, however, is a bit misleading, as it looks like the leftmost resonance peaks tail off and disappear as A/ω goes to zero. Looking at the equation for P_{SW} this should not be the case, and indeed it isn't. If we take a slice of the plot through $\varepsilon_0/\omega = 7$ then we see that the population is 0.5 as A/ω goes to zero as expected (see Fig. 5.4). The reason we do not see this on the full density plot is that the peaks become incredibly thin in this region, as we can see in the same figure by taking a slice perpendicular to the first at $A/\omega = 2$ and restricting ourselves to a small region around $\varepsilon_0/\omega = 7$. These

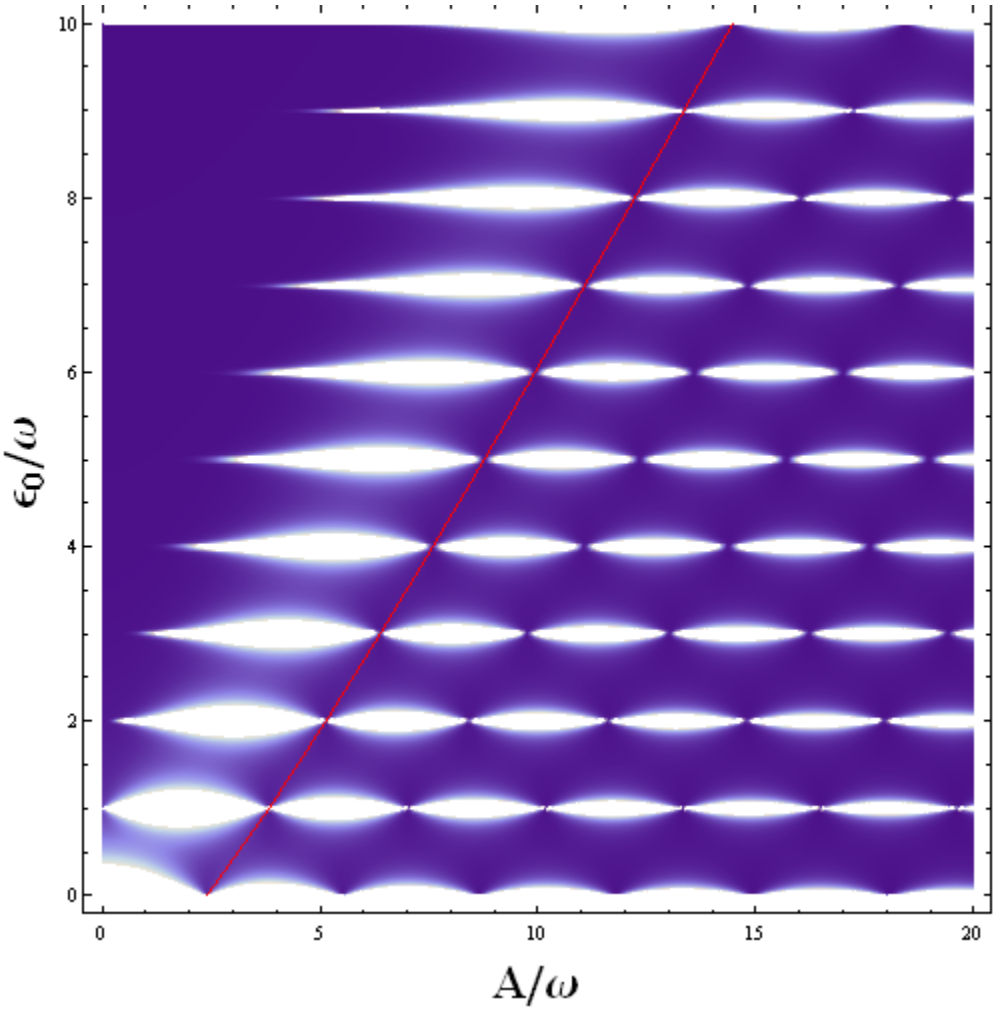

Figure 5.3: Density plot of time-averaged population of $|L\rangle$ as a function of A/ω and ε_0/ω for $\Delta = 0.01$. Purple regions correspond to populations near zero, and white to populations of 0.5. The red line plots n as a function of $j_{n,1}$, the first 0 of the n^{th}-order Bessel function to show dependence of the resonance peaks. This is our own reproduction of the data presented in [21].

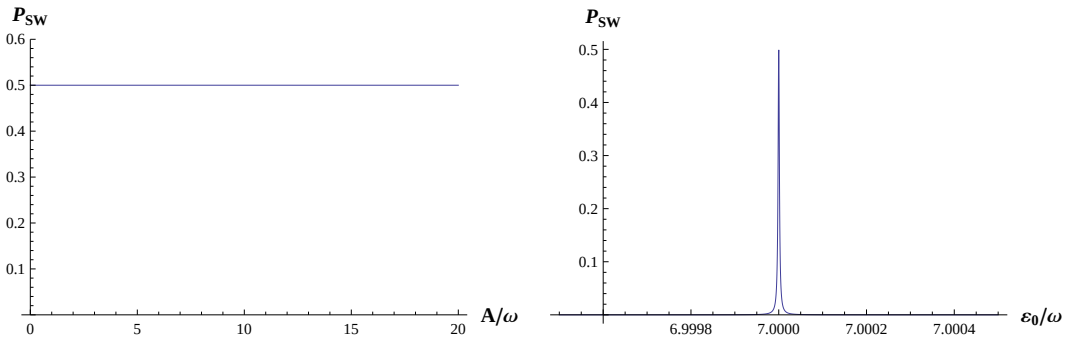

(a) (b)

Figure 5.4: Slices of P_{SW} in a region that appears to have 0 population in Fig. 5.3: (a) through $\varepsilon_0/\omega = 7$ and (b) through $A/\omega = 2$.

peaks are so thin, in fact, that the area under them approaches 0. A physical measurement is obtained by convolving the signal to be measured with the pulse from equipment performing the measurement (something like a Gaussian, say). If the area under the signal is 0, the convolution will also evaluate to 0, and we will not detect the spike even though the mathematics say it should be there. This highlights a fundamental difference between mathematics and physics, as no experiment could ever measure a peak with zero area. For our scheme to be viable, we must ensure that we do not stray into this region of infinitely sharp resonance peaks, which we can do by making A sufficiently large. Another consideration is the value of Δ. As stated before, we want P_{LZ} to be close to 1 so that we can be sure we are observing true constructive interference. In Fig. 5.5 we see that increasing Δ washes out the resonance peaks. Good contrast is key to distinguishing factors from nonfactors, so we must work with small Δ, which we take to be on the order of 0.01 for most calculations.

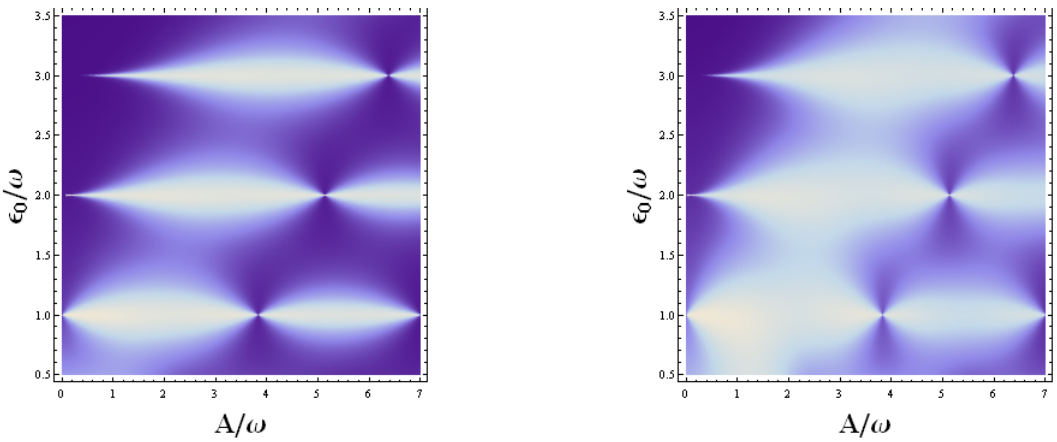

(a) (b)

Figure 5.5: Effect of increasing Δ on the sharpness of resonance peaks for (a) $\Delta = 0.5$ and (b) $\Delta = 1$.

We have explored, at least qualitatively, most of the relevant features of P_{SW}, but have yet to check it against the full numerical result obtained by direct integration of Schrödinger's equation. This was carried out over only half of the domain displayed in Fig. 5.3 due to the lengthy calculation time, but there is enough there to make the comparison. Fig. 5.6 demonstrates resonance peaks at integer values of ε_0/ω and coherent destruction of tunneling for A/ω corresponding to zeros of Bessel functions (the Bessel fit is not shown in this plot but we checked the values against it). Thus we can feel confident in using the analytical expression for P_{SW} when calculating quantities relevant to our factorization method.

5.2.3 A First Attempt: $\varepsilon_0 = N$

Now we turn to utilizing these multiphoton resonances as a means for factoring integers. Like with Gauss sums, this method is naïve in the sense that is a

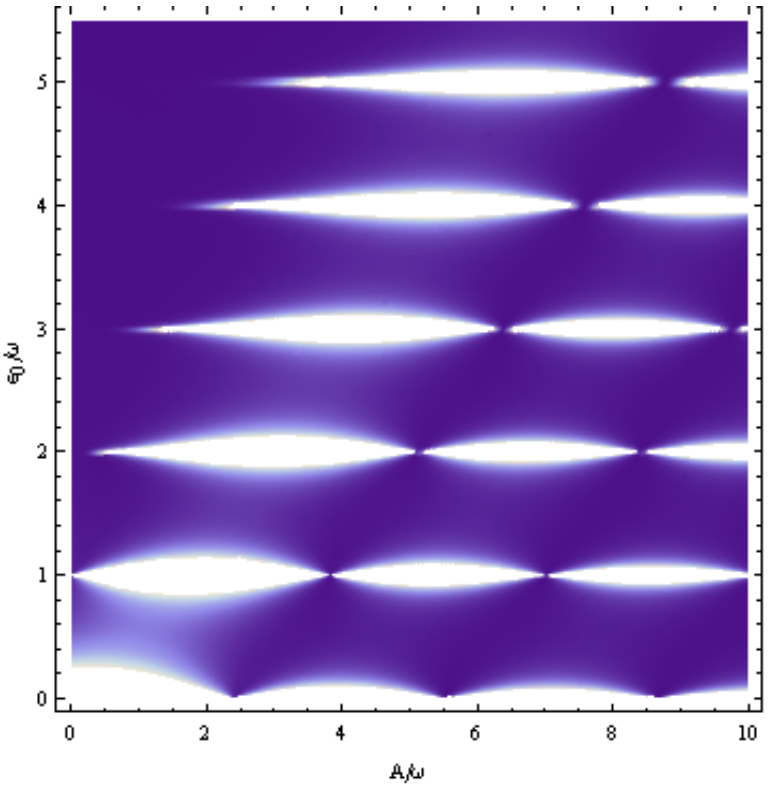

Figure 5.6: Density plot for the direct numerical calculation of P_{SW} for $\Delta = 0.01$, showing excellent agreement with the analytical expression.

factor tester and not truly an algorithmic factor finder. We took this approach in the hopes that quantum entanglement would allow us to test multiple factors simultaneously, and we will explore some potential ways of achieving this goal.

Looking at the resonance condition Eq. (5.6), the most obvious choice for setting up the problem is to set ε_0 equal to the composite number, N, and use ω to test if integers $l \in \left[7, \lfloor\sqrt{N}\rfloor\right]$ (we can tell at first glance whether or not a number has 2 and/or 5 as factors, and there exist efficient means to see if 3 is a factor) are factors of N. The brackets $\lfloor\ \rfloor$ denote the floor function, whose output is the greatest integer not greater than its argument. Note that we must also have $A \backsimeq N$ in order for LZ transitions to actually occur; if it were smaller than ε_0 the system would never pass through the avoided crossing.

The sharp resonance peaks displayed above suggest that factor testing is possible with this system. The important information comes with how the problem scales as a function of the size of the input. To get at this quantity, we look at the behavior of the average population as N increases. A typical plot of the average population as a function of transition number for the case of a factor is displayed in Fig. 5.7. We obtained the plot through the numerical solution of the differential equations governing the system, but we can get at more analytical behavior by considering Eq. (5.12). According to the sinsuoidal term of this equation, the excited state population will undergo coherent oscillations with frequency $\omega' = \sqrt{(\varepsilon_0 - n\omega)^2 + |\Delta_n|^2}$. When a number is a factor of N (and thus the Lorenztian prefactor is 1), the average

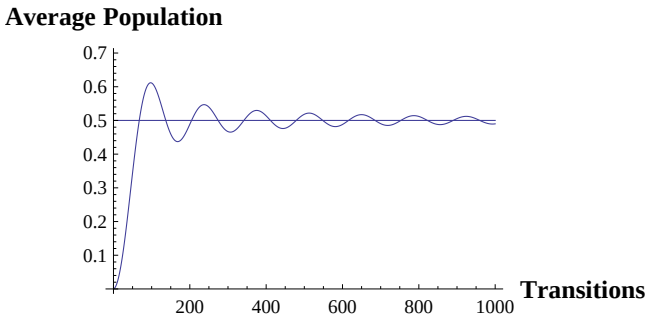

Figure 5.7: Average population as a function of transition number, for the parameters $\varepsilon_0 = 15$, $\omega = 5$, $A = 25$, and $\Delta = 0.1$.

population for an arbitrary number of transitions, l, is given by

$$f(l) = \frac{1}{l}\int_0^l \sin^2(\omega' t)\, dt\,. \tag{5.13}$$

We would like to solve this equation to find an explicit formula for the location of the first maximum, which is indicated by the purple line in Fig. 5.8. This would give us a reasonable measure for the time it takes to determine if a test factor actually is a factor. Unfortunately, the solutions for the maxima and minima are found by a transcendental equation:

$$\tan(2\omega' l) = 2\omega' l\,.$$

Rather than waste efforts calculating this quantity for each new case, we look to another measure of the computational time for finding a factor of our input number. A more easily calculable number is the time it takes for the instantaneous population of the excited state to reach 1: $t_1 = \pi/2\omega'$, the green vertical line in Fig. 5.8. Here the average population is already equal to 1/2, so we can

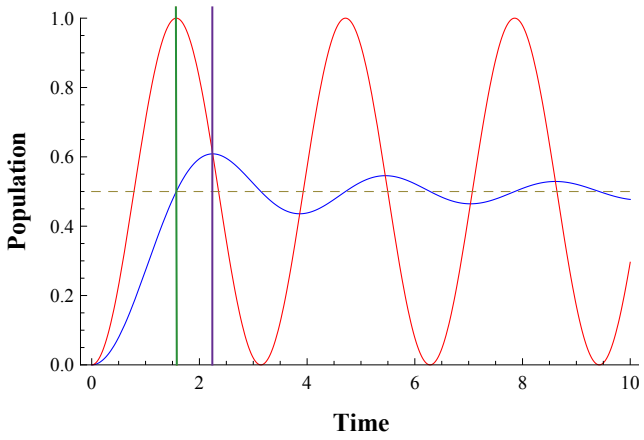

Figure 5.8: A plot of $\sin^2(\omega' t)$ (red) and its average value (blue) for $\omega' = 1$. The dashed horizontal line gives the asymptotic average population value of 0.5. The vertical green and purple lines display the two measures of time needed to distinguish a factor, maximum of the instantaneous population and maximum of the average population, respectively.

be reasonably sure that our trial integer is a factor (this is because the system undergoes coherent oscillation at resonance, resulting in a time-averaged population of 1/2 over many oscillations as in Fig. 5.7). When ω is factor of N, we are on resonance, and the $(\varepsilon_0 - n\omega)^2$ term drops out of ω'. This gives the following expression for t_1:

$$t_1 = \frac{\pi}{2|\Delta J_n(A/\omega)|}\,. \tag{5.14}$$

As a worst-case test, we assume that the input integer is a product of two primes close together so that there are no other primes in between them. Fig. 5.9 displays the calculation of t_1 for $\Delta = 0.01$, using our worst-case scenario for N. It shows, as expected, that the time to determine a factor increases with the problem size, but the exact scaling relationship is not obvious.

We can actually calculate a closed-form polynomial function for this data that will give us a scaling law for testing a single factor as the input number grows. Denoting the m^{th} prime as p_m, the input N is of the form $N = p_m p_{m+1}$. We also then have $A = p_m p_{m+1}$ (so that is on the order of ε_0 and LZ transitions actually occur), $\omega = p_m$, and, hence, $n = p_{m+1}$. Putting these values into Eq. (5.14), t_1 becomes $\pi/2|\Delta J_{p_{m+1}}(p_{m+1})|$. But p_m and p_{m+1} are relatively close to one another (the distance being roughly $\ln p_m$ according to the prime number theorem), so we can approximate both to be on the order of $\sqrt{N}$. We can therefore write the relevant timescale as

$$t_1 = \frac{\pi}{2|\Delta J_{\sqrt{N}}(\sqrt{N})|} \,. \tag{5.15}$$

Thus characterizing the behavior of t_1 as N grows depends on determining the asymptotic behavior of Bessel functions with the same argument and order. To find this behavior, we use the following expression for $J_n(x)$ for large n [22]:

$$J_n(x) = \left(\frac{2}{x}\right)^{1/3} \text{Ai}\left[\left(\frac{2}{x}\right)^{1/3} (n-x)\right] \,, \tag{5.16}$$

where $\text{Ai}(u) = \frac{1}{\pi}\int_0^\infty \cos(ut + \frac{1}{3}t^3)dt$ is the Airy function, a solution of the differential equation of the form $y'' - uy = 0$. In our case, we have $n = x = \sqrt{N}$ so that the Bessel function can be written

$$J_n(n) = \text{Ai}[0] 2^{1/3} N^{-1/6} \,, \tag{5.17}$$

with $\text{Ai}[0] = \frac{1}{3^{2/3}\Gamma\left(\frac{2}{3}\right)} \approx 0.355$ (Γ is again the Gamma function), a value

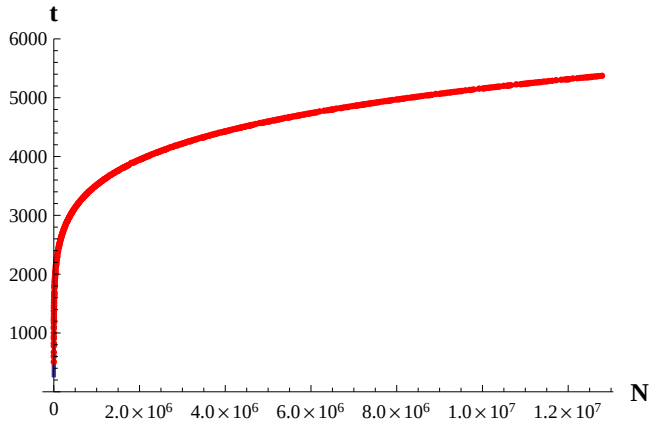

Figure 5.9: The time to distinguish a test factor as a function of the input number size for composite numbers of the form $p_m \cdot p_{m+1}$ and $\Delta = 0.01$, where p_m denotes the m^{th} prime number. The blue solid line shows the analytical fit given by Eq. (5.18), but it is hard to see behind the points.

obtained in Mathematica. Putting this all together, the final functional form of t_1 is

$$t_1 = \frac{\pi 3^{2/3} \Gamma\left(\frac{2}{3}\right)}{2^{4/3}\Delta} N^{1/6} \,. \tag{5.18}$$

This gives the time needed to identify a single number as a factor of N. Since we are testing close to all of the integers up to $\lfloor\sqrt{N}\rfloor$, there are on the order of $\sqrt{N}$ numbers for which we need to repeat the process. This takes the total processing time to $cN^{2/3}$, where c is a constant. Such a scaling relationship is better than that of the Gauss sum process, and on the order of a Kummer sum (see Appendix C).

One way to improve upon this scaling relationship is to test multiple trial factors at the same time. Because the trial factor is given by the drive frequency, ω, our only hope with the current scheme is to try a linear superposi-

tion of frequencies. To start we use a test drive of the form

$$f(t) = A(\cos(\omega t) + \cos(k\omega t)),$$

where k is a rational number. In the ideal case we would get information about both test factors, ω and $k\omega$ (ignoring for the moment that these cannot both be prime factors). We ran simulations for these bichromatic drives for values of $k = 3,\ 3/2,\ 4/3$, with the results presented in Fig. 5.10. The patterns of the resonance peaks become markedly more complicated, but there is a striking feature common to all three plots. The peaks now arise at integer multiples of $\varepsilon_0/q\omega$, where q is the denominator of the rational representation of k, in lowest terms. Thus for $k = 3$ the resonance peaks occur at the same values of ε_0 as the single-drive case, but for $k = 3/2$ and $k = 4/3$ we see peaks at every half-integer and one-third-integer multiple of ε_0/ω, respectively. This feature is the result of what are known as *generalized Bessel functions*, which can be expressed via a generating function [85]:[2]

$$e^{i\,(u\sin(\omega_1 t)+v\sin(\omega_2 t))} = \sum_{n=-\infty}^{\infty} J_n^{\omega_1,\,\omega_2}(u,\,v)e^{i\,nt}\,. \tag{5.19}$$

The authors of [86] demonstrate that if we have $k = p/q$ in lowest terms as above, then the generalized Bessel functions result in the resonance condition of $\varepsilon_0 = nq\omega$, which we observed in our simulations. This suggests that a linear superposition of two drive frequencies will not allow us to extract information

[2]Thanks to Professor Frederick Strauch of Williams College for directing us to the relevant literature regarding these functions.

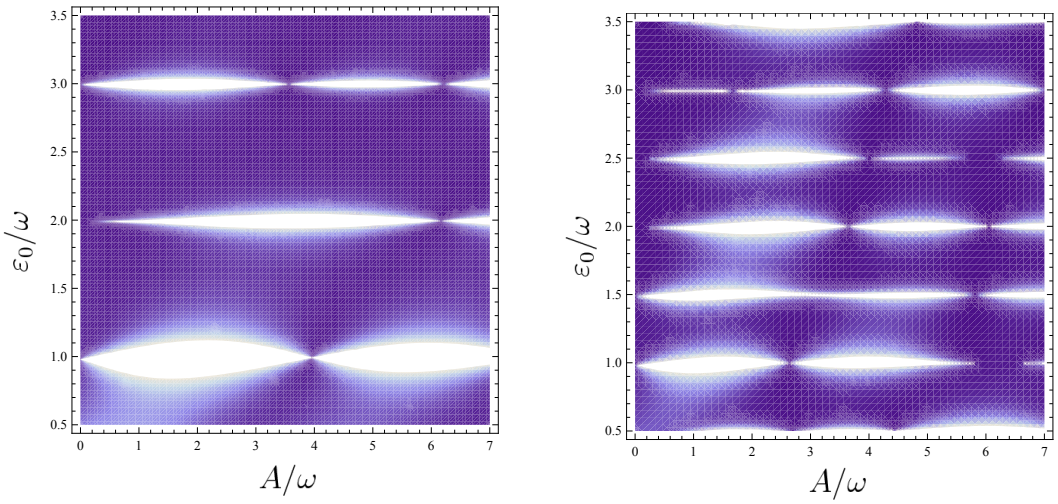

(a) k=3

(b) k=3/2

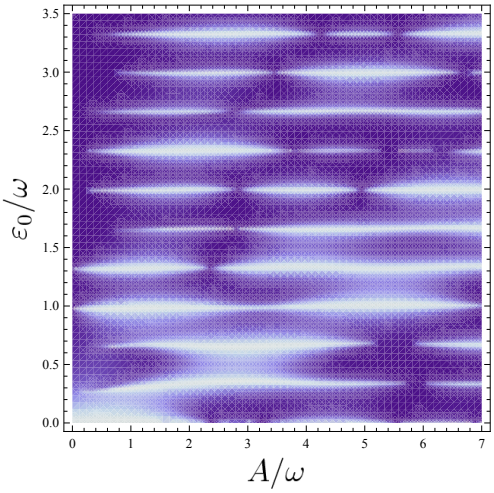

(c) k=4/3

Figure 5.10: Effect of two rationally-related drive frequencies on excited state population for different values of k.

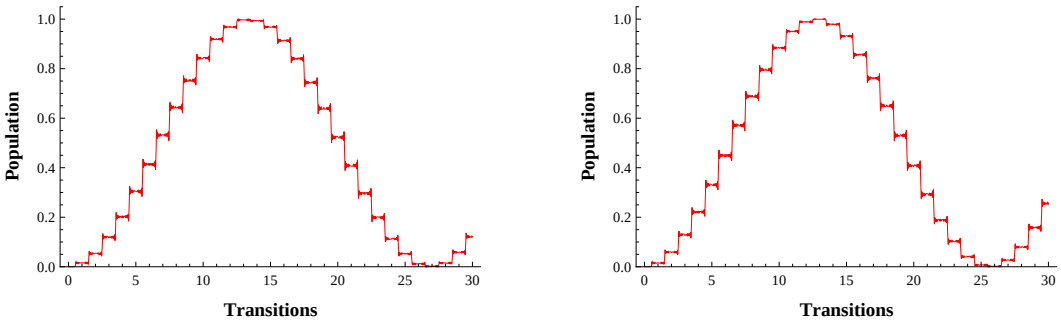

(a) $\varepsilon_0 = 1/5$ (b) $\varepsilon_0 = 3/5$

Figure 5.11: Testing that 5 is a factor of 15 using two different values of ε_0 that have the same denominator. While not identical, the two plots display coherent oscillations of population, illustrating the relevant information is contained with the denominator of ε_0

about both frequencies, and we must pursue a different way of setting up the problem.

5.2.4 A Second Method: $\omega = 1/N$

To be able to simultaneously test multiple factors, we flip the first method on its head. Now we assign the values $\omega = 1/N$ and $\varepsilon_0 = 1/l$, where N is the number to be factored and l is the factor to be tested. The test factor actually depends only on the denominator of ε_0 when written in lowest terms, as evidenced by Fig. 5.11, but for simplicity we will take the numerator to be 1. At first glance encoding the input integer number in ε_0 seems like a small change, but the flux detuning is a parameter that can be put into superpositions of two values in a properly constructed system. The idea is to perform repeated LZ transitions through two (or more) anticrossings, each with a separately controllable flux detuning.

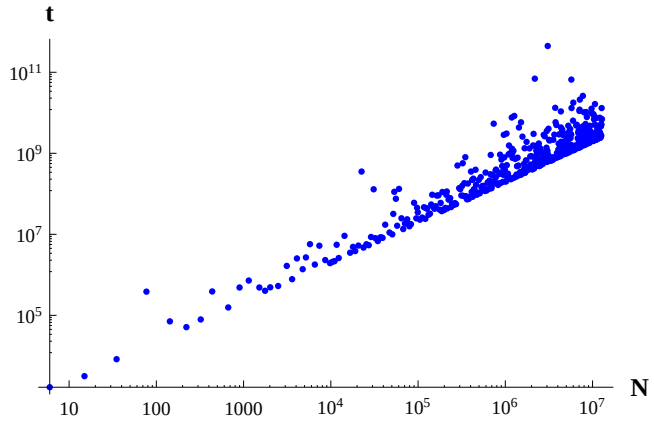

Figure 5.12: Log-log plot of t_1 for the case $\omega = 1/N$ and $\Delta = 0.01$, displaying the unpredictable behavior.

Because the flux detuning will decrease as we increase the test factor, one might think that we can similarly scale back the drive amplitude A to ensure repeated LZ transitions occur. We want to work in the diabatic limit, however, which requires that the sweep speed, $\sqrt{A\omega}$ be much larger than the tunnel splitting, Δ. But now the drive frequency scales as $1/N$, forcing A to scale as N to ensure that the diabaticity condition is met for Δ in the range $0.01 - 0.1$.

As of this writing, however, we have yet to determine a concrete scaling as we did for the case $\varepsilon_0 = N$. If we perform a similar analysis as above, the Bessel function component of t_1 behaves as

$$J_{\sqrt{N}}(N^2)\,. \tag{5.20}$$

This causes t_1 to have the erratic behavior displayed in Fig. 5.12, and as a result we have yet to find an expression for its asymptotic behavior. There is an added concern if we decrease the drive frequency (which will decrease with

increasing N) too much. As the MIT group notes in later papers [22, 25], if the frequency, ν, is roughly equal to the inverse of the dephasing rate, $1/T_2$, then the resonance condition is lost, and with it any hope of distinguishing between factors and nonfactors.

Though this setup suffers from potential scaling issues and physical constraints, it does allow us to simultaneously test more than one factor. Such multiple factor testing requires that there be more than two levels in the system since we will need more than one anticrossing. As we discussed in Chapter 2, Hilbert spaces combine via the tensor product, so n qubits create a Hilbert space of dimension 2^n. This expansion of the working Hilbert space is achieved through the coupling of qubits.

If we inductively couple two qubits via a tunable mutual inductor in between them, we can tune the interaction strength between the two working qubits by threading flux through the coupler (see Fig. 5.13) [87, 88].[3] The full, two-level Hamiltonian describing the situation in Fig. 5.13 becomes

$$H = \sum_{i=1,2} \left(\frac{\varepsilon_i}{2}\, \sigma_z^{(i)} + \Delta_i\, \sigma_x^{(i)} \right) + \frac{J}{2}\, \sigma_z^{(1)} \sigma_z^{(2)}\,, \tag{5.21}$$

where we can control the ε_i's by using inductors to apply magnetic flux to each qubit, J is the tunable coupling strength, and the notation $\sigma_j^{(i)}$ refers to the σ_j operator acting on the i^{th} qubit, as outlined in Section 2.2.1.

We plot the energy eigenstates of this Hamiltonian in Fig. 5.14, which illustrates a total of four anticrossings. As this factorization method is based

[3]More attention is paid to the coupling of qubits in Appendix D. For now we'll just assume that we can write the total Hamiltonian as we have.

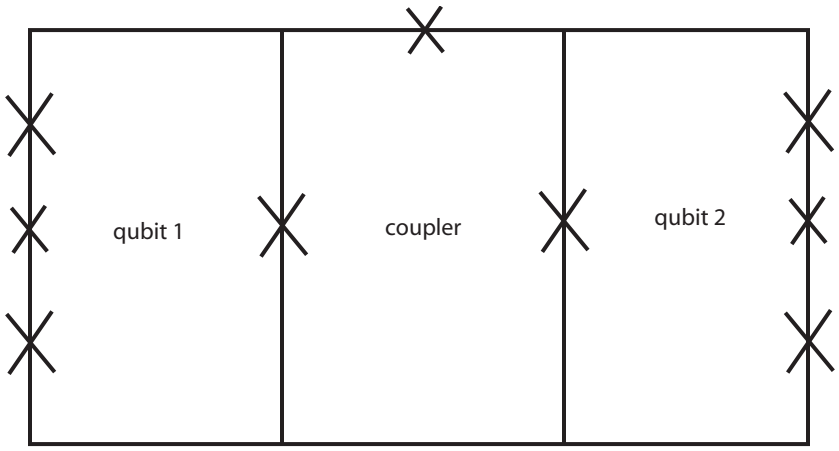

Figure 5.13: Schematic showing how two 3-junction flux qubits can be tunably coupled

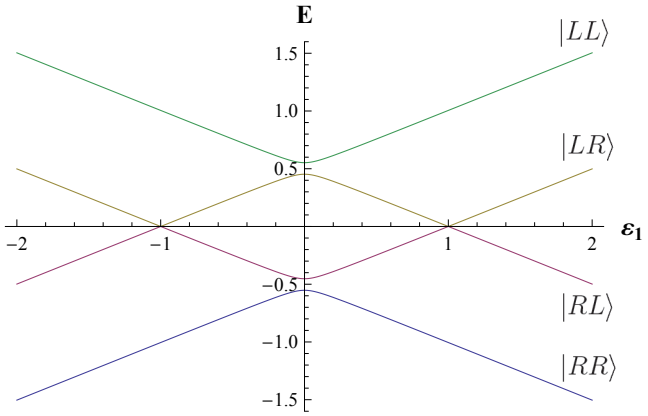

Figure 5.14: Plot of eigenenergies of the Hamiltonian Eq. (5.21) as a function of ε_1 for $\Delta_1 = 0.05$, $\Delta_2 = 0.05$, $\varepsilon_2 = 1$, and $J = 0$.

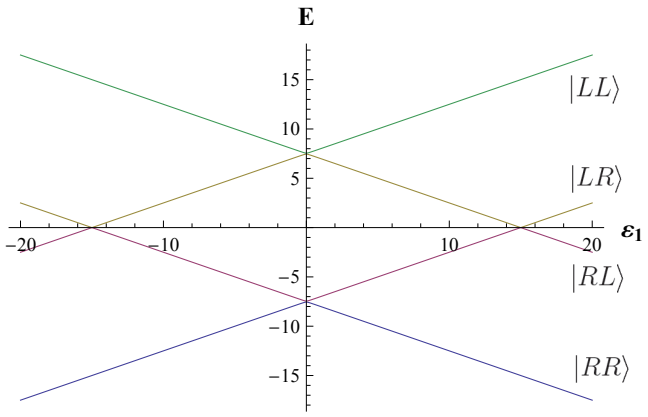

Figure 5.15: Plot of eigenenergies of the Hamiltonian Eq. (5.21) as a function of ε_1 for $\Delta_1 = 0.05$, $\Delta_2 = 0.05$, $\varepsilon_2 = 15$, and $J = 0$. The anticrossings are all moved away from the origin along both coordinate axes.

on repeated LZ transitions, ε_1 in the Hamiltonian becomes something of the form $\varepsilon_0 + A\cos(\omega t)$, so that we repeatedly sweep through the anticrossings. The dynamics of the problems are complicated if we traverse all four anticrossings, but we can increase ε_2, the static flux detuning of the second qubit, so that our drive keeps the system localized around only the center two if $A < \varepsilon_2$ (see Fig. 5.15 and note the change of scale). Because we have control over the coupling term via J and over the static flux detuning of qubit 1 via ε_0, we can move the two centrally located anticrossings. This is where we get the ability to test two factors simultaneously, by using the different detunings to represent two factors, l_1 and l_2.

We simplify the problem by assuming that we have $\varepsilon_0 > J$. This places the location of the two anticrossings at $-(\varepsilon_0 + J)$ and $-(\varepsilon_0 - J)$, as in Fig. 5.16. Thus if we set $\varepsilon_0 = 1/a$ and $J = 1/b$ with a, $b \in \mathbb{Z}^+$, the anticrossings will be at $-\left(\frac{b-a}{ab}\right)$ and $-\left(\frac{b+a}{ab}\right)$. The denominator of each of these numbers in reduced

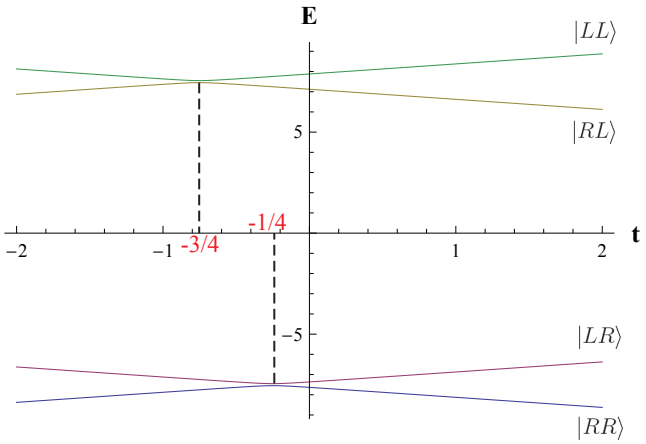

Figure 5.16: Energy diagram for the two qubit Hamiltonian (with $\varepsilon_1 = \varepsilon_0 + t$) as a function of time with parameters $\varepsilon_0 = 1/2$, $\Delta_1 = 0.05$, $\Delta_2 = 0.05$, $\varepsilon_2 = 15$, and $J = 1/4$. The vertical dashed lines have been inserted to highlight the locations of the anticrossings, which correspond to $-(J + \varepsilon_0)$ and $-(\varepsilon_0 - J)$.

form gives the factors to be tested. The problem has thus been reduced to one of algebra, where we try to pick a and b such that we can produce pairs of primes. It appears, however, that finding a and b for an arbitrary pair of primes cannot always be done if a and b are integers.

By instead letting ε_0 and J be rational numbers, we allow ourselves an extra degree of freedom. Now we can create arbitrary pairs of primes by the following process. Let our two primes be denoted p and q, and without loss of generality assume that p is less than q. We seek integers m and n (again, without loss of generality, let's assume $n > m$) such that $m + n = q$ and $n - m = p$. Thus if we set $\varepsilon_0 = n/pq$ and $J = m/pq$ we have

$$\varepsilon_0 + J = \frac{n}{pq} + \frac{m}{pq} = \frac{n+m}{pq} = \frac{q}{pq} = \frac{1}{p} \tag{5.22}$$

and

$$\varepsilon_0 - J = \frac{n}{pq} - \frac{m}{pq} = \frac{n-m}{pq} = \frac{p}{pq} = \frac{1}{q}\,, \tag{5.23}$$

which sets our anticrossings to be at the inverses of our two primes, as desired. Finding m and n is straightforward, and we obtain

$$n = \frac{q+p}{2} \text{ and } m = \frac{q-p}{2}\,, \tag{5.24}$$

which are always integers since q and p are odd. As an illustration of this scheme, we demonstrate in Figs. 5.17 and 5.18 that we can simultaneously test 7 and 11 as factors by letting $\varepsilon_0 = 9/77$ and $J = 2/77$ ($n = 9$ and $m = 2$). We observe small amplitude oscillations even when either 7 or 11 is not a factor of the input number, which is likely due to the fact that in each case the test integers are close to being actual factors (e.g. 7 is a factor of 21, which is close to 22). We could make these smaller by decreasing Δ further so that the resonances are sharper. This increased resolution comes at the price of increasing the time it takes to resolve a factor, as evidenced by Eq. (5.18).

For each simulation, we prepare the system in the state $\frac{1}{\sqrt{2}}\left(|LL\rangle + |LR\rangle\right)$, so that the first qubit is in state $|L\rangle$ and the second in $\frac{1}{\sqrt{2}}\left(|L\rangle + |R\rangle\right)$ (note that in practice this would require that we apply a Hadamard gate to the second qubit to obtain the equal superposition). Because we have set up the problem such that LZ transitions occur only at the two slightly off-center anticrossings, population oscillations are restricted to two disjoint sets of states, $\{|LL\rangle\,, |RL\rangle\}$ and $\{|LR\rangle\,, |RR\rangle\}$, as illustrated in Figs. 5.17 and 5.18.

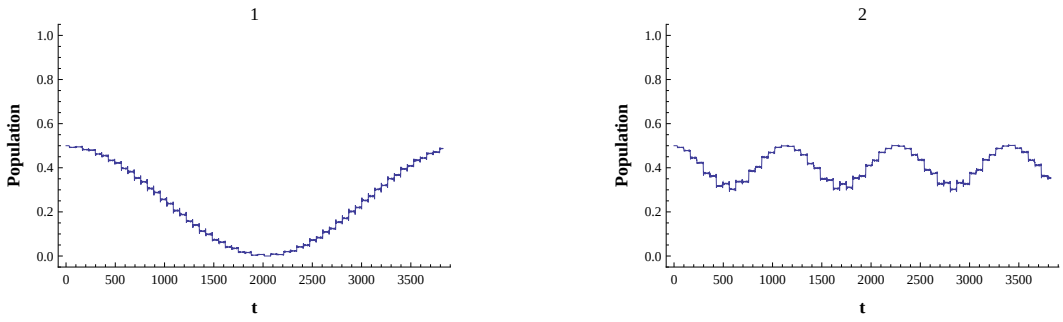

(a) $|LL\rangle$ (b) $|LR\rangle$

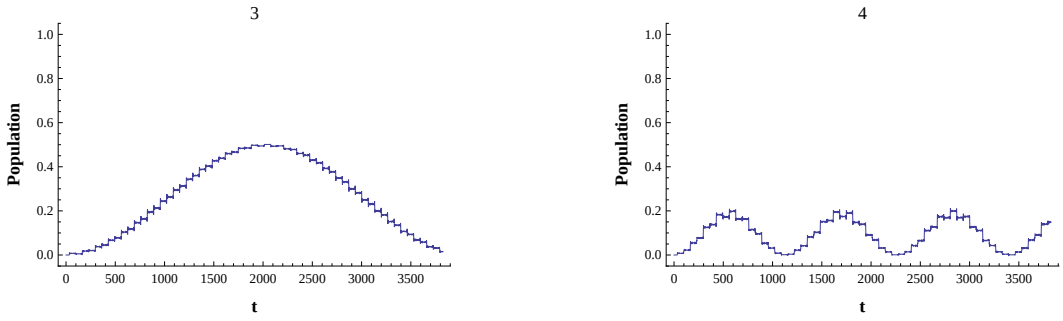

(c) $|RL\rangle$ (d) $|RR\rangle$

Figure 5.17: Testing if 7 and 11 are factors of 21, with parameters $\Delta = 0.05$ and $A = 21$. The full oscillations in $|LL\rangle$ and $|RL\rangle$ and the lack of full oscillations in $|LR\rangle$ and $|RR\rangle$ signify that 7 is a factor while 11 is not.

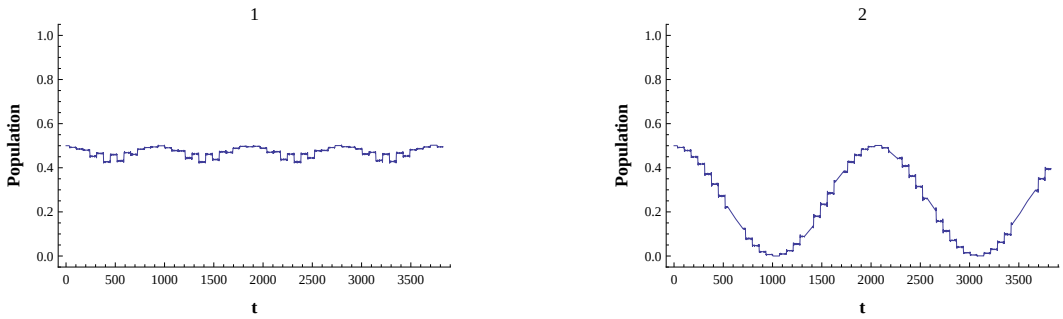

(a) $|LL\rangle$ (b) $|LR\rangle$

(c) $|RL\rangle$ (d) $|RR\rangle$

Figure 5.18: Testing if 7 and 11 are factors of 22, with parameters $\Delta = 0.05$ and $A = 22$. The full oscillations in $|LR\rangle$ and $|RR\rangle$ and the lack of full oscillations in $|LL\rangle$ and $|RL\rangle$ signify that 11 is a factor while 7 is not.

This demonstration suggests that we can simultaneously test whether or not two prime numbers are factors within a system of coupled superconducting qubits. We have displayed the scheme only for two prime numbers tested against two different input integers, but the method has been verified for various other cases. The next step is to try this for larger and larger numbers to make sure that we can still differentiate factors from nonfactors with good fidelity. We want to derive a concrete scaling law for multiple factor testing, as it might be different than the single-qubit case (which is still undefined for $\omega = 1/N$). Because ω is getting smaller and smaller as N gets larger, there is likely a point where the multiphoton resonances are no longer excited, as observed by the group at MIT. After deriving this scaling law, we would like to expand this method to 3 qubits in the hopes we can simultaneously test $4 = 2^2$ factors, thus achieving good scaling of resources.

Chapter 6

Conclusions and Future Work

This thesis presents a factorization method based on repeated LZ transitions. We have built up the theory from the basics of two-level systems and from the LZ problem as first posed in 1932. By expounding on recent experiments that observed interference from repeated LZ transitions, we propose that the resonance condition for multiphoton transitions can be used to determinine whether or a not an integer is a factor of another number. That method on its own is computationally inefficient, scaling as $O(N^{2/3})$ in the size of the input number N. This is comparable to a similar scheme called Gauss sum factorization, which has garnered recent theoretical and experimental interest [36].

We have demonstrated that it is possible to use coupled qubits to perform simultaneous factor testing by inducing repeated LZ transitions through two anticrossings. Using external dc fluxes, we can precisely control the location of the anticrossings relative to the symmetry point of our harmonic drive. These

two anticrossings give us two different resonance conditions, which equates to testing two different prime numbers as factors of N. While the problem still scales exponentially, this is, to our knowledge, the first diffraction-based proposal that uses entanglement to test multiple factors.

The past year has been a fruitful time of learning and discovery, and the latest results that simulate multiple factor testing are particularly exciting. But, as is the case with any scientific research, many questions remain unanswered. In the following sections we outline some of the open problems to direct possible future research in this area.

6.1 Extending the Transfer Matrix Method

In Chapter 4 we presented the transfer matrix formulation of repeated LZ transitions. While we demonstrated the power of this method, we did not end up using it in later simulations. This was due to difficulties in extending it to the case of nonzero ε_0, which changed the dynamical phases in a nontrivial way. Though we have an idea of how to change the matrices to fit the more general case, so far the transfer matrix method has not matched the exact numerics. From a computational standpoint, it would be desirable to resolve this issue since Mathematica's NDSolve runs slowly when the problem parameters and integration times become large. Though the matrix multiplication is not trivial, it is more efficient than directly solving the differential equations and would allow us to more easily probe larger input numbers.

6.2 Exponential Sums

Because both methods have their basis in diffraction, it is tempting to draw parallels between Gauss sum factorization and factorization via repeated LZ transitions. At the moment the precise relationship is not fully understood. It is not clear if there is a one-to-one correspondence between the two or if their connection begins and ends at diffraction. Should there be a strong relationship, then one avenue worth exploring would be what is known as an "exponential sum." The term Gauss sum refers only to sums of quadratic phase factors, and sums with different exponents have different names (see Appendix C). Exponential sums over an index m have phase factors proportional to m^m. It can be shown that this makes the scaling law logarithmic in N, a significant step towards an efficient algorithm (it doesn't get you everything though, because you still need to test on the order of $\sqrt{N}$ factors). Finding a way of carrying out exponential sums with repeated LZ transtions could be a potentially rewarding direction for future research.

6.3 Randomization

In the Gauss sum method of factorization, one must complete a sum over all the integers between 1 and $\sqrt{N}$. Practical limitations prevent this from being a viable task, so all experimental realizations to date have had to truncate the sum after a smaller number of terms. Because they are now sampling phase factors over a very limited range of the unit circle, the interference is not complete and the differentiation between factors and non-factors is not

ideal. To combat this problem, researchers have proposed and tested a method that randomly samples a small number of terms of the sum between 1 and $\sqrt{N}$ [75, 76, 79]. This way they still do not have to carry out a full Gauss sum but manage to hit more of the unit circle. Simulations and experiments alike have shown that this method improves the scaling law and increases the contrast between factors and nonfactors. It is possible that there might be some form of randomization within our system that would improve factor testing. One potential parameter to randomize is the energy splitting, Δ, which we could randomly set for each pass through the anticrossing. It remains to be seen whether or not this has any practical advantage.

6.4 More Qubits = More Factors?

We have demonstrated that coupling two qubits allows for the simultaneous testing of two factors. In order to be an efficient scheme, we want the number of factors tested to scale exponentially with the number of qubits. By this we mean that if we have an N qubit system, we should be able to test 2^{N-1} factors at the same time. The exponent is $N-1$ rather than N because we essentially pushed half of the anticrossings aside. The next step is to test the simulations for 3, 4, 5,... qubits to see if the method still works. The numerical simulations will likely become intractable rather quickly since the Hilbert space increases exponentially. Once the relationship has been established numerically for a few small cases, an analytical study of the general N-qubit case would be desired.

It would also be worth exploring the full system Hamiltonian rather than the two-level approximation we've made here. It's possible that adding more qubits or driving the system harder (which would be needed to factor larger numbers) will place more constraints on our parameter space. Stronger driving equates to putting more energy into the system, which might excite the state out of the lowest energy levels.

Appendix A

Tensor Products

We mentioned in Chapter 2 that as a result of the tensor product, a n-qubit system will have a Hilbert space of dimension 2^n. Generally following the discussion of tensor products given in [37], we will demonstrate the mechanism behind this growth of Hilbert space size. A visualization of how to perform this multiplication will make clearer how to represent matrices like $\sigma_x^{(1)}$.

We begin with two vector spaces V and W of dimension m and n, respectively, and a field F (in our case V and W are Hilbert spaces and F is $\mathbb{C}$, the complex numbers). The tensor product, $\otimes$, is an operation on these vector spaces that satisfies the following properties:

1. Given $c \in \mathbb{C}$ and vectors $|v\rangle \in V$, $|w\rangle \in W$, then

$$c(|v\rangle \otimes |w\rangle) = (c\,|v\rangle) \otimes |w\rangle = |v\rangle \otimes (c\,|w\rangle)\,. \tag{A.1}$$

2. Given $|v_1\rangle$, $|v_2\rangle \in V$ and $|w\rangle \in W$, then

$$(|v_1\rangle + |v_2\rangle) \otimes |w\rangle = |v_1\rangle \otimes |w\rangle + |v_2\rangle \otimes |w\rangle \ . \tag{A.2}$$

3. Given $|v\rangle \in V$ and $|w_1\rangle$, $|w_2\rangle \in W$, then

$$|v\rangle \otimes (|w_1\rangle + |w_2\rangle) = |v\rangle \otimes |w_1\rangle + |v\rangle \otimes |w_2\rangle \ . \tag{A.3}$$

This is more easily visualized if we consider the tensor product of matrices representing linear operators on vector spaces, which is known as the Kronecker product. Given $m \times n$ and $p \times q$ matrices

$$A = \begin{pmatrix} a_{00} & \cdots & a_{0n} \\ \vdots & \ddots & \vdots \\ a_{m0} & \cdots & a_{mn} \end{pmatrix}$$

and

$$B = \begin{pmatrix} b_{00} & \cdots & b_{0q} \\ \vdots & \ddots & \vdots \\ b_{p0} & \cdots & b_{pq} \end{pmatrix} \ ,$$

we define their Kronecker product $\otimes$ by

$$A \otimes B = \begin{pmatrix} a_{00}B & \cdots & a_{0n}B \\ \vdots & \ddots & \vdots \\ a_{m0}B & \cdots & a_{mn}B \end{pmatrix}$$

$$= \begin{pmatrix} a_{00}b_{00} & a_{00}b_{01} & \cdots & a_{00}b_{0q} & \cdots & a_{0n}b_{00} & a_{0n}b_{01} & \cdots & a_{0n}b_{0q} \\ \vdots & \vdots & \ddots & \vdots & \ddots & \vdots & \vdots & \ddots & \vdots \\ a_{00}b_{p0} & a_{00}b_{p1} & \cdots & a_{00}b_{pq} & \cdots & a_{0n}b_{p0} & a_{0n}b_{p1} & \cdots & a_{0n}b_{pq} \\ \vdots & \vdots & \ddots & \vdots & \ddots & \vdots & \vdots & \ddots & \vdots \\ a_{m0}b_{00} & a_{m0}b_{01} & \cdots & a_{m0}b_{0q} & \cdots & a_{mn}b_{00} & a_{mn}b_{01} & \cdots & a_{mn}b_{0q} \\ \vdots & \vdots & \ddots & \vdots & \ddots & \vdots & \vdots & \ddots & \vdots \\ a_{m0}b_{p0} & a_{m0}b_{p1} & \cdots & a_{m0}b_{pq} & \cdots & a_{mn}b_{p0} & a_{mn}b_{p1} & \cdots & a_{mn}b_{pq} \end{pmatrix}.$$

Thus the Kronecker product of a $m \times n$ matrix with a $p \times q$ matrix yields a $mp \times nq$ matrix.

As an example, consider the gate σ_x acting on the first qubit:

$$\sigma_x^{(1)} = \sigma_x \otimes I = \begin{pmatrix} 0 & 1 \\ 1 & 0 \end{pmatrix} \otimes \begin{pmatrix} 1 & 0 \\ 0 & 1 \end{pmatrix} = \begin{pmatrix} 0 & 0 & 1 & 0 \\ 0 & 0 & 0 & 1 \\ 1 & 0 & 0 & 0 \\ 0 & 1 & 0 & 0 \end{pmatrix}.$$

Note that CNOT,

$$\begin{pmatrix} 1 & 0 & 0 & 0 \\ 0 & 1 & 0 & 0 \\ 0 & 0 & 0 & 1 \\ 0 & 0 & 1 & 0 \end{pmatrix},$$

cannot be written as a tensor product of two single-qubit gates and is thus a good gate for creating entangled states.

Appendix B

The Interaction Picture

In Section 4.2.1 we mentioned the interaction picture when we wrote out the full state for our two-level system. This is a simply a different way to describe a quantum state than we normally see in undergraduate quantum mechanics, but it contains the same information. A typical undergraduate QM course presents the Schrödinger picture, which places all time-dependence within the states themselves by way of the time evolution operator:

$$|\psi(t)\rangle = e^{-i\,Ht/\hbar}\,|\psi(0)\rangle\ , \tag{B.1}$$

where H is the system's Hamiltonian.

The other end of the spectrum, the Heisenberg picture, completely shifts the time-depedence to the operators themselves. Taking the time derivative of an observable, O, we obtain the equation (see, e.g., [84])

$$\frac{d}{dt}O = \frac{i}{\hbar}\,[H,\,O] + \frac{\partial O}{\partial t}\,. \tag{B.2}$$

The interaction picture is a third, intermediate picture that splits the time-dependence between the operators and the states [89]. We break the Hamiltonian into two parts, one time-dependent and the other time-independent: $H = H_0 + V$, with V being the time-dependent perturbation. We define the interaction state vector as

$$|\psi_I(t)\rangle = e^{i\,H_0 t/\hbar}\,|\psi_S(t)\rangle \tag{B.3}$$

where $|\psi_S(t)\rangle$ is the state vector from the Schrödinger picture in Eq. (B.1). The new effective Hamiltonian becomes

$$V_I(t) = e^{i\,H_0 t/\hbar}\,V\,e^{-i\,H_0 t/\hbar}, \tag{B.4}$$

so that we have the equation of motion for the new states:

$$i\,\hbar\frac{d\,|\psi_I(t)\rangle}{dt} = V_I\,|\psi_I(t)\rangle\ . \tag{B.5}$$

An arbitrary operator, O, in the Schrödinger picture is governed by the transformation

$$O_I = e^{i\,H_0 t/\hbar}\,O\,e^{-i\,H_0 t/\hbar}. \tag{B.6}$$

We see that both the operators and the state vectors now carry some of the time-dependence. Sometimes the dominant term of the Hamiltonian, H_0 by construction, is time-dependent, as was true in Section 4.2.1 (here the σ_x term was the perturbation since Δ was small compared to ω and A). In that case,

we replace factors of the form $e^{\pm i\, H_0 t/\hbar}$ with

$$\exp\left[\pm\frac{i}{\hbar}\int_0^t H_0\, dt'\right]\,. \tag{B.7}$$

Appendix C

Gauss Sums

In this Appendix we present, without derivation, some of the key results from Gauss sum factorization. A few simulations provide a visible demonstration of how they work and highlight some relevant properties. The scenarios for these simulations are not my own, and the figures are reproductions of results in [78] and [82].

C.1 Fourier, Gauss, Kummer,...

The term Gauss sum refers to a special case of the more general exponential sum, defined by

$$\mathcal{A}_N^{(\ell-1,j)}(\ell) \equiv \frac{1}{\ell} \sum_{m=0}^{\ell-1} \exp\left[2\pi i\, m^j \frac{N}{\ell}\right] . \tag{C.1}$$

The value of j determines what type of sum this is, with $j = 1$ being the normal Fourier sum, $j = 2$ being the Gauss sum, and $j = 3$ being the Kummer sum [78]. Thus if we let N be the number we want to factor and ℓ be the trial

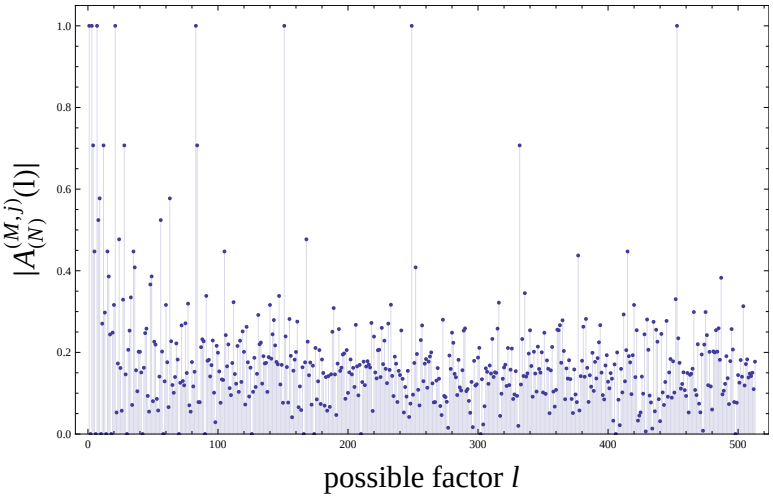

Figure C.1: A Gauss sum for $N = 263193$ and $M = 30$.

factor, then the terms in the sum will add constructively if ℓ is a factor of N and destructively otherwise. In practice, the sum must be truncated after a small number of terms, M, yielding the truncated exponential sum:

$$\mathcal{A}_N^{(M,j)}(\ell) \equiv \frac{1}{M+1} \sum_{m=0}^{M} \exp\left[2\pi i\, m^j \frac{N}{\ell}\right] . \tag{C.2}$$

The quantity $|\mathcal{A}_N^{(M,j)}(\ell)|$ will be equal to 1 if ℓ is a factor of N.

C.2 Ghost Factors and Randomization

Fig. C.1 displays a Gauss sum performed for $N = 263193 = 3 \cdot 7 \cdot 83 \cdot 151$, with the sum taken to $M = 30$ terms. The prime factors, and their integer multiples, are clearly visible as their associated signals are unity. There are, however, some nonfactors whose signals are rather high, at roughly 0.7 (in some situations the signal of a nonfactor can be even closer to 1). These

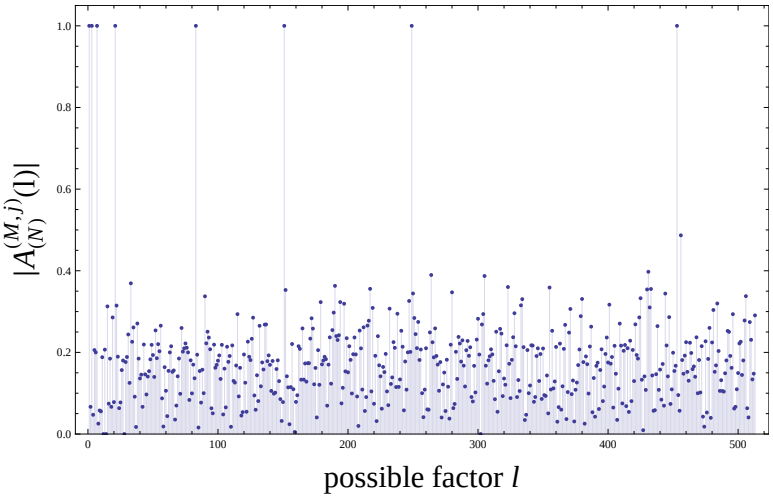

Figure C.2: A Gauss sum for $N = 263193$, $M = 30$, and random sampling.

factors are called ghost factors and can pose problems depending upon the resolution of the experiment.

One way to surpress these ghost factors is to take a random sample of the terms over which you sum [75, 76, 79]. The terms in the sum in Eq. (C.2) all lie on the complex unit circle, their distribution determined in part by the value of j. If we sum the terms in sequential order, we are sampling complex numbers in the same region of the unit circle so that their destructive interference won't be complete in the case of a nonfactor. If we instead use a random sampling of m's, there is an increased likelihood the terms of the sum will be more evenly distributed about the unit circle. The effect is illustrated in Fig. C.2, where the sum was carried out for $M = 30$ but with random sampling of m.

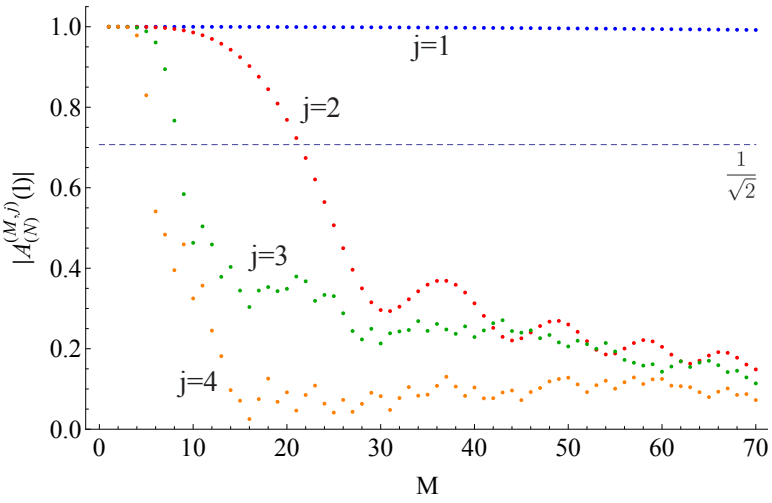

Figure C.3: The signal for one trial factor plotted as a function of truncation parameter, M, for various values of j. The input number is $10^6 + 1$, and the trial factor is 1000. This presents a worst-case test since 1000^2 is so close to N. The dashed horizontal line indicates the threshold value of $1/\sqrt{2}$.

C.3 Scaling laws and j

The measure of efficiency for this algorithm is how many terms of the truncated sum are needed so that a nonfactor is suppressed. In [78] the general scaling relationship for quenching a nonfactor below a desired threshold is given to be $O(N^{1/2j})$ for a given j. So increasing j leads to faster suppression of nonfactors, as illustrated in Fig. C.3. This, unfortunately, is still exponential in the input size, but in the same paper the authors find a scaling law for the truly exponential case $j = m$. They find through numerical simulations that only on the order of $\ln\sqrt{N}$ terms of the truncated sum are needed to determine the factors of N. Achieving an exponential sum as opposed to a normal Gauss sum is much more difficult in practice, but a group has made a first step towards realizing this scheme in a Bose-Einstein condensate [90].

Appendix D

Coupling Qubits

Coupling of superconduting qubits is typically achieved via a capacitor or an inductor, depending on qubit type. For charge and phase qubits, capacitors are used to give a fixed coupling between the charge states of the two qubits [91, 92]. This creates a 4-state charge basis in which to work, allowing for the implementation of 2-qubit gates.

Since flux states form the basis for flux qubits, we manipulate them using magnetic fields, and thus inductors are the likely candidates for a coupling scheme. This method of coupling was first outlined by Orlando *et al.* in their original proposal for persistent-current (flux) qubits [60] and finally realized experimentally in 2004 [93]. A fixed coupling scheme can be realized through the mutual inductance between two flux qubits placed close together, resulting in an interaction Hamiltonian of the form

$$H_{12} = \alpha_1 \sigma_z^{(1)} \sigma_z^{(2)} \,, \tag{D.1}$$

where α_1 is a coupling constant.

As mentioned in the text, we can make this interaction strength a tunable parameter by using a third loop in between the two qubits. The authors of [88] derive an expression for that parameter, J, given by

$$J(\phi_c) = \frac{\hbar}{e} \frac{I'(\phi_c)}{I_c^2 - I(\phi_c)^2} I_{p1} I_{p2} \,, \tag{D.2}$$

where ϕ_c is the flux threaded through the coupler loop, I_c is the critical current through the junctions on the vertical edges of the coupler loop (see Fig. 5.13), $I(\phi_c) = I_c \sin\bar{\phi}$ ($\bar{\phi}$ is the phase across each of those two junctions), and I_{pi} is the persistent current through the i^{th} qubit.

Bibliography

[1] R. Feynman, International Journal of Theoretical Physics **21**, 467 (1982).

[2] D. Deutsch, Proceedings of the Royal Society of London. Series A, Mathematical and Physical Sciences **400**, 97 (1985).

[3] D. Deutsch and R. Jozsa, Proceedings of the Royal Society of London. Series A, Mathematical and Physical Sciences **439**, 553 (1992).

[4] P. W. Shor, in *The 35th Annual IEEE Symposium on Foundations of Computer Science* (IEEE Computer Society Press, Sante Fe, NM, 1994), pp. 124–134.

[5] L. K. Grover, Physical Review Letters **79**, 325 (1997).

[6] Y. Makhlin, G. Schön, and A. Shnirman, Reviews of Modern Physics **73**, 357 (2001).

[7] L. Landau, Phys. Z. Sowjet. **2**, 46 (1932).

[8] C. Zener, Proceedings of the Royal Society of London. Series A, Mathematical and Physical Sciences **137**, 696 (1932).

[9] E. C. G. Stückelberg, Helvetica Physica Acta **5**, 369 (1932).

[10] Y. Kayanuma, Physical Review B **47**, 9940 (1993).

[11] Y. Kayanuma, Physical Review A **50**, 843 (1994).

[12] Y. Kayanuma, Physical Review A **55**, R2495 (1997).

[13] Y. Kayanuma and Y. Mizumoto, Physical Review A **62**, 061401 (2000).

[14] Y. Kayanuma, Applied and Computational Mathematics **6**, 143 (2007).

[15] Y. Kayanuma and K. Saito, Physical Review A **77**, 010101R (2008).

[16] B. M. Garraway and N. V. Vitanov, Physical Review A **55**, 4418 (1997).

[17] A. Izmalkov, M. Grajcar, E. Il'chev, N. Oukhanski, T. Wagner, H.-G. Meyer, W. Krech, M. H. S. Amin, A. Maassen van den Brink, and A. M. Zagoskin, Europhysics Letters **65**, 844 (2004).

[18] M. Sillanpää, T. Lehtinen, A. Paila, Y. Makhlin, and P. Hakonen, Physical Review Letters **96**, 187002 (2006).

[19] M. Sillanpää, T. Lehtinen, A. Paila, Y. Makhlin, and P. Hakonen, Journal of Low Temperature Physics **146**, 253 (2007).

[20] A. Paila, J. Tuorila, M. Sillanpää, D. Gunnarsson, J. Sarkar, Y. Makhlin, E. Thuneberg, and P. Hakonen (2009), URL `arXiv:0901.1304`.

[21] W. D. Oliver, Y. Yu, J. C. Lee, K. K. Berggren, L. S. Levitov, and T. P. Orlando, Science **310**, 1653 (2005).

[22] D. M. Berns, W. D. Oliver, S. O. Valenzuela, A. V. Shytov, K. K. Berggren, L. S. Levitov, and T. P. Orlando, Physical Review Letters **97**, 150502 (2006).

[23] D. M. Berns, M. S. Rudner, S. O. Valenzuela, K. K. Berggren, W. D. Oliver, L. S. Levitov, and T. P. Orlando, Nature **455**, 51 (2008).

[24] M. S. Rudner, A. V. Shytov, L. S. Levitov, D. M. Berns, W. D. Oliver, S. O. Valenzuela, and T. P. Orlando, Physical Review Letters **101**, 190502 (2008).

[25] W. D. Oliver and S. O. Valenzuela, Quantum Information Processing **8**, 261 (2009).

[26] D. A. Garanin and R. Schilling, Europhysics Letters **59**, 7 (2002).

[27] C. Hicke, L. F. Santos, and M. I. Dykman, Physical Review A **73**, 012342 (2006).

[28] V. G. Benza and G. Strini, Fortschritte Der Physik-Progress of Physics **51**, 14 (2003).

[29] K. Saito, M. Wubs, S. Kohler, P. Hanggi, and Y. Kayanuma, Europhysics Letters **76**, 22 (2006).

[30] D. Zueco, G. M. Reuther, P. Hanggi, and S. Kohler (2008), URL `arXiv:0812.4253v1`.

[31] M. Wubs, S. Kohler, and P. Hanggi, Physica E **40**, 187 (2007).

[32] E. Farhi, J. Goldstone, S. Gutmann, J. Lapan, A. Lundgren, and D. Preda, Science **292**, 472 (2001).

[33] S. Ashhab, J. R. Johansson, and F. Nori, Physical Review A **74**, 6 (2006).

[34] J. Johansson, M. H. S. Amin, A. J. Berkley, P. Bunyk, V. Choi, R. Harris, M. W. Johnson, T. M. Lanting, S. Lloyd, and G. Rose (2008), URL `arXiv:0807.0797v1`.

[35] J. F. Clauser and J. P. Dowling, Physical Review A **53**, 4587 (1996).

[36] W. Merkel, I. S. Averbukh, B. Girard, G. C. Paulus, and W. P. Schleich, Fortschritte der Physik **54**, 856 (2006).

[37] M. A. Nielsen and I. L. Chuang, *Quantum Computation and Quantum Information* (Cambridge University Press, Cambridge, 2000).

[38] P. Kaye, R. Laflamme, and M. Mosca, *An Introduction to Quantum Computing* (Oxford University Press, Oxford, 2007).

[39] C. H. Bennett, G. Brassard, C. Crepeau, R. Jozsa, A. Peres, and W. K. Wootters, Physical Review Letters **70**, 1895 (1993).

[40] R. Raussendorf and H. J. Briegel, Physical Review Letters **86**, 5188 (2001).

[41] A. Ekert, Physica Scripta **T76**, 218 (1998).

[42] D. P. DiVincenzo, in *Mesoscopic Electron Transport*, edited by L. L. Sohn, L. P. Kouwenhoven, and G. Schön (Kluwer, Dordrecht, 1997), pp. 657–677.

[43] J. I. Cirac and P. Zoller, Physical Review Letters **74**, 4091 (1995).

[44] E. Knill, R. Laflamme, and G. J. Milburn, Nature **409**, 46 (2001).

[45] D. G. Cory, A. F. Fahmy, and T. Havel, in *PhysComp '96* (Boston, MA, 1996), pp. 87–91.

[46] Y. Nakamura, C. D. Chen, and J. S. Tsai, Physical Review Letters **79**, 2328 (1997).

[47] Y. Nakamura, Y. A. Pashkin, and J. S. Tsai, Nature **398**, 786 (1999).

[48] V. Bouchiat, D. Vion, P. Joyez, D. Esteve, and M. H. Devoret, Physica Scripta Volume T **76**, 165 (1998).

[49] J. R. Friedman, V. Patel, W. Chen, S. K. Tolpygo, and J. E. Lukens, Nature **206**, 43 (2000).

[50] C. H. van der Wal, A. C. J. ter Haar, F. K. Wilhelm, R. N. Schouten, C. Harmans, T. P. Orlando, S. Lloyd, and J. E. Mooij, Science **290**, 773 (2000).

[51] T. P. Orlando and K. A. Delin, *Foundations of Applied Superconductivity* (Addison-Wesley, Reading, 1991).

[52] M. Tinkham, *Introduction to Superconductivity* (Dover Publications, Mineola, 2004), 2nd ed.

[53] K. K. Likharev, *Dynamics of Josephson Junctions and Circuits* (Gordon and Breach, New York, 1986).

[54] S. Han, in *Exploring the Quantum/Classical Quantum Frontier*, edited by J. R. Friedman and S. Han (Nova Science Publishers, New York, 2003), pp. 59–95.

[55] A. Cottet, PhD thesis, The University of Paris 6 (2002).

[56] J. Diggins, T. D. Clark, H. Prance, R. J. Prance, T. P. Spiller, J. Ralph, and F. Brouers, Physica B **215**, 367 (1995).

[57] J. Diggins, R. Whiteman, T. D. Clark, R. J. Prance, H. Prance, J. F. Ralph, A. Widom, and Y. N. Srivastava, Physica B **233**, 8 (1997).

[58] R. Rouse, S. Han, and J. E. Lukens, Physical Review Letters **75**, 1614 (1995).

[59] T. P. Orlando, *Two-Level System with Static and Dynamical Coupling* (2004).

[60] T. P. Orlando, J. E. Mooij, L. Tian, C. H. van der Wal, L. S. Levitov, S. Lloyd, and J. J. Mazo, Physical Review B **60**, 15398 (1999).

[61] J. E. Mooij, T. P. Orlando, L. Levitov, L. Tian, C. H. van der Wal, and S. Lloyd, Science **285**, 1036 (1999).

[62] F. G. Paauw, A. Federov, C. J. P. M. Harmans, and J. E. Mooij (2008), URL `arXiv:0812.1912v1`.

[63] C. Wittig, Journal of Physical Chemistry B **109**, 8428 (2005).

[64] E. T. Whittaker and G. N. Watson, *A Course in Modern Analysis* (Cambridge University Press, Cambridge, 1927), 4th ed.

[65] F. Grossmann and P. Hanggi, EPL **18**, 571 (1992).

[66] S. Ashhab, J. R. Johansson, A. M. Zagoskin, and F. Nori, Physical Review A **75**, 063414 (2007).

[67] M. Wubs, K. Saito, S. Kohler, Y. Kayanuma, and P. Hanggi, New Journal of Physics **7**, 218 (2005).

[68] K. Saito and Y. Kayanuma, Physical Review B **70**, 201304 (2004).

[69] K. Mullen, E. Benjacob, Y. Gefen, and Z. Schuss, Physical Review Letters **62**, 2543 (1989).

[70] D. A. Garanin and R. Schilling, Physical Review B **66**, 11 (2002).

[71] A. V. Shytov, D. A. Ivanov, and M. V. Feigel'man, Eur. Phys. J. B **36**, 263 (2003).

[72] K. Blum, *Denisty Matrix Theory and Applications* (Plenum Press, New York, 1996), 2nd ed.

[73] D. M. Bressoud, *Factorization and Primality Testing*, Undergraduate Texts in Mathematics (Springer-Verlag, New York, 1989).

[74] J. Summhammer, Physical Review A **56**, 4324 (1997).

[75] X. Peng and D. Suter, EPL **84** (2008).

[76] M. Mehring, K. Miller, I. S. Averbukh, W. Merkel, and W. P. Schleich, Physical Review Letters **98**, 120502 (2007).

[77] M. Stefanak, W. Merkel, W. P. Schleich, D. Haase, and H. Maier, New Journal of Physics **9**, 370 (2007).

[78] M. Stefanak, D. Haase, W. Merkel, M. S. Zubairy, and W. P. Schleich, Journal of Physics A: Mathematical and Theoretical **41**, 304024 (2008).

[79] S. Weber, B. Chatel, and B. Girard, EPL **83**, 34008 (2008).

[80] T. S. Mahesh, N. Rajendran, X. H. Peng, and D. Suter, Physical Review A **75**, 4 (2007).

[81] D. Bigourd, B. Chatel, W. P. Schleich, and B. Girard, Physical Review Letters **100** (2008).

[82] M. Gilowski, T. Wendrich, T. Muller, C. Jentsch, W. Ertmer, E. M. Rasel, and W. P. Schleich, Physical Review Letters **100** (2008).

[83] A. A. Rangelov, Journal of Physics B: Atomic, Molecular and Optical Physics **42**, 021002 (2009).

[84] D. J. Griffiths, *Introduction to Quantum Mechanics* (Pearson Prentice Hall, Upper Saddle River, 2004), 2nd ed.

[85] H. J. Korsch, A. Klumpp, and D. Witthaut, Journal of Physics A: Mathematical and General **39**, 14947 (2006).

[86] A. Klumpp, D. Witthaut, and H. J. Korsch, Journal of Physics A: Mathematical and Theoretical **40**, 2299 (2007).

[87] A. O. Niskanen, K. Harrabi, F. Yoshihara, Y. Nakamura, S. Lloyd, and J. S. Tsai, Science **316**, 723 (2007).

[88] S. H. W. van der Ploeg, A. Izmalkov, A. Maassen van den Brink, U. Hubner, M. Grajcar, E. Il'ichev, H. G. Meyer, and A. M. Zagoskin, Physical Review Letters **98**, 4 (2007).

[89] E. Merzbacher, *Quantum Mechanics* (John Wiley & Sons, Inc., New York, 1970), 2nd ed.

[90] M. Sadgrove, S. Kumar, and K. Nakagawa, Physical Review Letters **101**, 180502 (2008).

[91] Y. A. Pashkin, T. Yamamoto, O. Astafiev, Y. Nakamura, D. V. Averin, and J. S. Tsai, Nature **421**, 823 (2003).

[92] A. J. Berkley, H. Xu, R. C. Ramos, M. A. Gubrud, F. W. Strauch, P. R. Johnson, J. R. Anderson, A. J. Dragt, C. J. Lobb, and F. C. Wellstood, Science **300**, 1548 (2003).

[93] A. Izmalkov, M. Grajcar, E. Il'ichev, T. Wagner, H. G. Meyer, A. Y. Smirnov, M. H. S. Amin, A. M. van den Brink, and A. M. Zagoskin, Physical Review Letters **93**, 4 (2004).